The Techno-Economic Potential of Power to Gas for Synthetic Natural Gas Production through Biogas Upgrading

by

Sogol Mottaghi-Tabar

A thesis

presented to the University of Waterloo

in fulfillment of the

thesis requirement for the degree of

Master of Applied Science

In

Chemical Engineering

Waterloo, Ontario, Canada, 2019

Author's Declaration

This thesis consists of material all of which I authored or co-authored: see Statement of Contributions included in the thesis. This is a true copy of the thesis, including any required final revisions, as accepted by my examiners.

I understand that my thesis may be made electronically available to the public.

Statement of Contributions

The information enclosed in sections 3 and 4 of this thesis have been incorporated within the following publications:

Robert Currie, Sogol Mottaghi-Tabar, Yichen Zhuang and David S. A. Simakov, "Design of an Actively Cooled Sabatier Reactor for Thermo-catalytic Hydrogenation of CO_2: Model-Based Feasibility Analysis and Experimental Proof-of-Concept". Published in the Journal of Industrial & Engineering Chemistry Research. Publication Date: July 1, 2019. DOI: 10.1021/acs.iecr.9b01426.

Sogol Mottaghi-Tabar, Robert Currie, Dave Thompson and David S. A. Simakov, "Techno-Economic Potential of Power to Gas for Synthetic Natural Gas Production through Biogas Upgrading". In process of submission.

Abstract

Raw biogas can be upgraded to produce pipeline grade synthetic natural gas (SNG) via thermo-catalytic hydrogenation of CO_2. This method reduces green house gas (GHG) emissions through offsetting fossil natural gas consumption while providing a financially profitable avenue for private sector investment. The H_2 needed for the system is generated via water electrolysis using surplus or inexpensive electricity. This study assesses the economic feasibility of constructing a SNG production facility for landfill gas upgrading via thermocatalytic hydrogenation of CO_2. A power-to-gas (PtG) setup is utilized to produce a comprehensive process flow diagram consisting of actively cooled heat exchanger type methanation reactors, alkaline electrolysers and auxiliary process units. The overall system is simulated in steady state using Aspen HYSYS to provide process stream specifications and utility requirements. Base equipment costs obtained from the chemical process model allow generation of further economic outlooks to determine feasible scenarios for the technology. Factors including payout period, net present worth and internal rate of return are calculated and show that profitable outcomes highly depend on the price of electricity and selling price of SNG. Production cost range from \$13-45/GJ with electricity prices in the \$0.04/kWh to \$0.18/kWh range. SNG selling prices at or above \$20/GJ are found to be necessary in order to provide economic scenarios attractive to investors.

Acknowledgements

I would like to thank my supervisor, Professor David Simakov for his mentorship, guidance and support throughout my masters program.

I would also like to thank my committee members: Professor Michael Fowler and Professor Eric Croiset for their time and contributions.

Special thanks to my group members Robert Currie, Yichen Zhuang, Guanjie Sun, Carol Yu and Muhammad Waqas Iqbal. Without their dedication and hard work, this project wouldn't have been possible.

A special thanks to Walker Industries and Professional Engineer Dave Thompson whose support and contributions were crucial to the successful completion of this work.

Lastly, thank you to my family for their support and encouragement through my academic journey.

Table of Contents

List of Figures

List of Tables

Abbreviations

SNG   synthetic natural gas

TOS   time-on-stream

PtG   power to gas

RWGS   reverse water gas shift

CCS   carbon capture and storage

MSR   methane steam reforming

MDR   methane dry reforming

FTS   Fischer-Tropsch synthesis

MS   methanol synthesis

DMS   direct methanol synthesis

SR   Sabatier reaction

WGS   water gas shift

Si   siloxanes

VOC   volatile organic compounds

LFG   landfill gas

PBR   packed bed reactor

STHE   shell and tube heat exchanger

TSA   temperature swing adsorption

PSA   pressure swing adsorption

AEL   alkaline electrolyser

PEM   polymer electrolyte membranes

SOEC   solid oxide electrolysis

BMC   base modular cost

FCI   fixed capital investment

TCI   total capital investment

ES   engineering supervision

C   construction

CF   contractor fee

Ct   contingency

CCF   cumulative cash flow

CF   cash flow

IRR   internal rate of return

NPW   net present worth

OC   operational cost

PAT   profit after tax

PBT   profit before tax

PC   production cost

PL   plant life

PW   present worth

Symbols

$a_{c,HE}$ cooling tube surface-to-volume ratio, m^{-1}

$a_{r,HE}$ cooling tube surface-to-packed volume ratio, m^{-1}

$a_{r,HL}$ reactor surface-to-volume ratio, m^{-1}

A_c total cross-sectional area of cooling tubes, m^2

A_j pre-exponential factor of the rate coefficient of reaction j, units of k_j

B_j pre-exponential factor of the adsorption coefficient of species i, units of K_j

C_i molar concentration of species i, mol/m^3

C_t total molar concentration, mol/m^3

C_{pc} coolant heat capacity, kJ/(kg K)

C_{pg} gas heat capacity, kJ/(mol K)

d wall thickness, m

d_p catalytic pellet diameter, m

D diameter, m

D_{ae} effective axial diffusion coefficient, m^2/s

D_m gas molecular diffusivity, m^2/s

E_j	activation energy of reaction j, kJ/mol
F	flow rate, mol/year
Ft	Ft factor
G_c	gravimetric (mass) flow rate of coolant, kg/s
h_{nc}	natural convection heat transfer coefficient, kJ/(m^2 s K)
h_w	effective wall heat transfer coefficient, kJ/(m^2 s K)
i	discount rate
H	enthalpy, kJ/mol
ΔH_i	adsorption enthalpy change of species i, kJ/mol
HHV	high heating value, GJ/mol
k_{ae}	effective axial thermal conductivity, kJ/(m s K)
k_j	rate constant of reaction j
K_i	adsorption constant of species i, bar^{-1}
$K_{j,eq}$	equilibrium constant of reaction j
L	reactor length, m
M	mass flow rate, kg/h
Nu	Nusselt number

p_i	partial pressure of gaseous species i, bar
P	pressure, bar
Pr	Prandtl number
P_{tf}	total feed gas pressure, bar
Q	heat flow, kJ/h
Q_{loss}	heat loss, kJ/h
Q_{leak}	heat leak, kJ/h
Re	Reynolds number
R_j	rate of reaction j, mol/(kg s)
R_g	gas constant, kJ/(mol K)
SV	space velocity, h^{-1}
S	selectivity
t	time, s
T	reactor temperature, K
T_c	coolant temperature, K
T_e	environment temperature, K
U_w	overall effective wall heat transfer coefficient, kJ/(m^2 s K)

v_g	gas velocity, m/s
V	compartment volume, m^3
W	work, J
X	conversion
Y	yield
y_i	mole fraction of i
z	reactor length coordinate, m

Greek letters

α_{ij}	stoichiometric coefficient of species i in reaction j
ε	catalyst bed porosity
ϕ	Thiele modulus
η_j	effectiveness factor of reaction j
λ	thermal conductivity, kW/(m K)
μ	viscosity, kg/(m s)
ρ_c	coolant density, kg/m^3
ρ_g	gas molar density, mol/m^3
ρ_s	solid density, kg/m^3
τ_b	catalyst bed tortuosity

Subscripts

air	compressed air
PBR	packed bed reactor
PB	packed bed
c	coolant
eff	effective
eq	equilibrium
f	feed
g	gas
HE	heat exchange
HL	heat loss
int	initial
nc	natural convection
out	outlet fluid
p	pellet
s	solid
r	reactor
in	inlet fluid
cold	cold fluid

hot	hot fluid
LMTD	log mean temperature difference
Util	utility fluid

1. Introduction

1.1.   *Problem statement and motivation*

Rapid industrialization and rise in atmospheric CO_2 demand innovative solutions for reduction of these emissions. Amongst these solutions are improving energy efficiency, transitioning to lower carbon energy sources, and CO_2 capture for sequestration or conversion into synthetic fuels and chemicals. Synthetic natural gas (SNG) production via CO_2 rich feedstock has attracted significant interest in recent years. Proposals by Union Gas and Enbridge Gas have aimed for targets of 2% SNG in the Canadian utility system by 2025 and 10% by 2030 [1]. In addition, Canadian Biogas Association and the Canadian Gas Association have proposed to have pipeline SNG contents of 5% by 2025 and 10% by 2030 [1]. Feasible processes will result in the reduction of greenhouse gas emissions, aid in resource recovery and provide an economically attractive platform for private sectors investment into the circular economy [1]. Pre-exiting pipeline gas infrastructure, vastly available for storage and transportation of the product, can help bring future SNG gas production to established markets.

Utilization of CO_2 as precursor for synthesizing fuels and chemicals has been extensively reviewed in literature [2, 3]. Reduction of CO_2 can be achieved through photochemical, electrochemical, or thermocatalytic means. Photochemical and electrochemical pathways show solubility and transport limitations [4]. Thermo-catalytic conversion via the highly exothermic Sabatier reaction, Eq.1, shows promise by combining high temperatures with heterogeneous catalysis leading to large reaction rates [4]. This reaction is typically accompanied by the reverse water gas shift (RWGS) and CO methanation shown in Eq.2 and Eq.3 respectively [4]. Water electrolysis, Eq.4, provides the required H_2 for the system.

$$CO_2 + 4H_2 \rightleftharpoons CH_4 + 2H_2O \qquad\qquad \Delta H^{\circ}_{298} = -164.9\ kJ/mol \qquad\qquad (1)$$

$$CO + 3H_2 \rightleftharpoons CH_4 + H_2O \qquad\qquad \Delta H^{\circ}_{298} = -206.1\ kJ/mol \qquad\qquad (2)$$

$$CO_2 + H_2 \rightleftharpoons CO + H_2O \qquad\qquad \Delta H^{\circ}_{298} = +41.2\ kJ/mol \qquad\qquad (3)$$

$$2H_2O \leftrightarrow O_2 + 2H_2 \qquad\qquad \Delta G = 237.23\ kJ/mol\ H_2O \qquad\qquad (4)$$
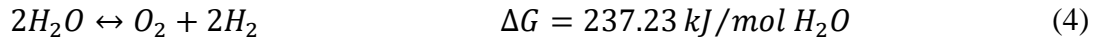
The highly exothermic nature of the methanation reaction can have adverse effects on reactor performance. High temperatures are unfavorable to the exothermic and reversible methanation process and accelerate catalyst deactivation [4]. Additionally, a suitable carbon source is required for feasible execution of the system.

A power to gas (PtG) system can be utilized to practically implement methanation at an industrial scale. Technologies for PtG systems show promise as a feasible means of connecting the electricity grid to the gas grid. The intermittent nature of renewable energy has set off a search for methods of electricity storage. An attractive avenue within PtG is SNG production due to abundant pre-existing natural gas infrastructure for storage and distribution [5]. In this study, a comprehensive methanation system is designed to produce pipeline grade synthetic natural gas accompanied by a feasibility analysis.

1.2. Project Objectives

Economic feasibility of power to gas (PtG) systems has been significantly investigated in recent years. Further work is required to increase its potential for widespread implementation. With technology development and up and coming reactor configurations, outlooks for the PtG system feasibility are on a rise. This work consists of 3 distinct sections:

1. A transient mathematical model of an actively cooled heat exchanger type packed bed Sabatier reactor was designed and investigated by numerical simulations to optimize CO_2 conversion and CH_4 production.

2. A comprehensive process was synthesized around the packed bed reactor to address the unique challenges associated with the feed carbon source and methanation reaction. Steady state process simulation strategies were utilized to specify all material and energy streams associated with the system. Where necessary, equipment design and sizing were performed providing basic capital requirements for process equipment.

3. The techno-economic feasibility of the PtG system using a single-pass actively cooled packed bed reactor was determined for a range of conditions using basic economic parameters such as internal rate of return (IRR), payback period and net present worth (NPW). This section includes a brief analysis on the feasibility of onsite electricity generation via renewable sources.

1.3.   Thesis Outline

This thesis contains a study on the techno economic feasibility of a power to gas system for synthetic natural gas production from biogas. Thesis chapters are summarized as follows:

Chapter 2 provides a review of recent literature on power to gas systems, thermocatalytic reactions, methanation catalysts, reactor configurations and techno-economic models for methanation.

Chapter 3 outlines the methodology used in the study for both reactor design, process synthesis, mathematical simulations and economic modelling.

Chapter 4 presents detailed results obtained in the study including the process flow diagrams, mathematical modelling outputs and economic results for a variety of cases.

Chapter 5 provides concluding remarks on the study with additional discussion on future work needed. All references used in this study can be found listed in Chapter 6.

2. Literature Review

2.1.   Thermocatalytic Conversion

Current strategies for CO_2 mitigation rely heavily on carbon capture and storage (CCS). These separation technologies include amine scrubbing, pressure swing adsorption and membrane separation followed by cryogenic liquefaction [4]. High purity streams of CO_2 can be utilized for enhanced oil recovery or stored underground. Technologies involving CCS require high economic investments in both capital and operation. Underground storage of CO_2 is restricted by geology and long-term effects are not well understood [6]. An alternative path is conversion of CO_2 to hydrocarbon fuels and chemicals. Using this approach, waste CO_2 can be recycled back into to energy sector as a hydrocarbon alleviating marginal demand from conversional fossil sources. The non-flammable, non-corrosive, non-toxic and abundant nature of CO_2 makes this chemical an ideal reactant [4]. Industrial processes synthesizing urea, salicylic acid and polycarbonates currently utilize CO_2 as a reactant [4]. Sources of concentrated CO_2 gas are abundant in today's fossil fuel driven economy. These include, but are not limited to flue gas from coal/natural gas power plants, off gas from chemical plants and biogas from landfills. These waste gases are generally flared or vented to atmosphere [4].

Conversion to fuels and chemicals has gained substantial interest in recent year. Main catalytic systems studied include photochemical reduction, electrochemical reduction and thermocatalytic conversion [4]. Photochemical and electrochemical reduction reactions have shown great promise in production of formic acid and methanol. These reaction systems utilize water, CO_2 and energy as their starting materials achieving a simplicity, which lends to be their greatest advantage. However, photochemical paths are limited by solar energy utilization while electrochemical paths

5

are limited by low efficiencies of electricity utilization. Both processes are hindered by low solubility of CO_2 in water at low temperatures and diffusion limitations [4]. Thermocatalytic conversion is promising as it combines heterogeneous catalysis with high temperatures leading to fast reaction rates and large production volumes [4]. Many thermocatalytic pathways have been discovered for synthesis of fuels and chemicals. These are illustrated in Figure 1.
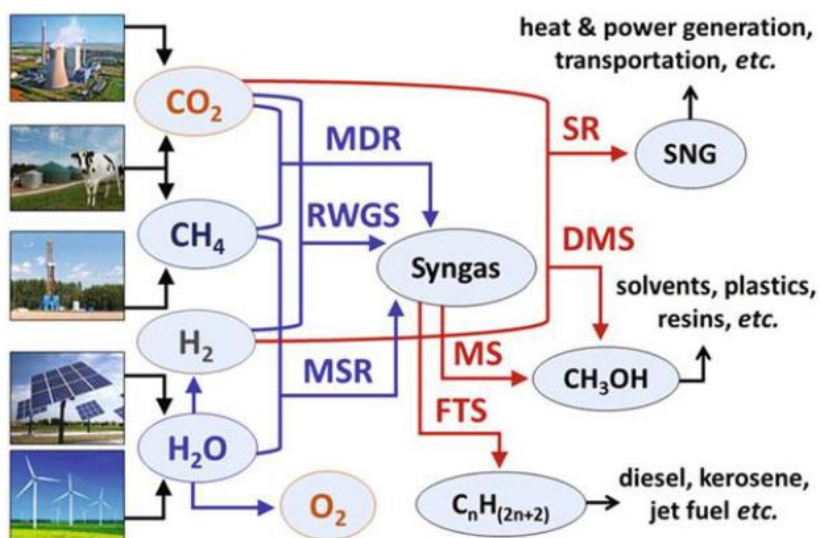
Figure 1. Thermocatalytic reaction pathways of synthesis of fuels and chemicals. Blue arrows are representative of endothermic reactions; red arrows are representative of exothermic reactions. Reactions include methane steam reforming (MSR), methane dry reforming (MDR), reverse water gas shift (RWGS), Fischer-Tropsch synthesis (FTS), methanol synthesis (MS), direct methanol synthesis (DMS), and the Sabatier reaction (SR) [4].

Most thermocatalytic reactions require H_2 gas as a reactant. Current hydrogen production at an industrial scale is achieved through methane steam reforming and water gas shift (WGS) reactions. The MSR reaction uses CH_4 as reactant and the WGS reaction produces CO_2 as a by-product. It

would be counterproductive to use either MSR or WGS reactions to fulfill the hydrogen requirements of a methanation system [4]. A promising technology for hydrogen production is water electrolysis, which utilizes electrochemical cells to produce high purity hydrogen and oxygen gas. Energy provided to the cells in the form of electricity will become renewable as the electrical grid switches to renewable sources. Off peak or surplus electricity can also be utilized for hydrogen production as a part of a PtG setup [4].

2.2.   Methanation

Natural gas currently holds key significance in the energy and transportation industry. Global infrastructure networks have been constructed for natural gas storage and distribution to industrial, commercial and residential sectors. Current natural gas sources are fossil based with extraction techniques including a variety of drilling and fracturing operations. The finite nature of fossil fuels paired with increased attention to green house gas emissions has sparked interest in synthetic natural gas (SNG) technologies. Methanation of carbon oxide rich gases is a promising path for SNG production [7]. Discovered by Sabatier and Senderens in 1902, methanation was initially used to remove CO from syngas in processes such as ammonia production [7]. Specifically, CO and H_2 were paired in an exothermic reaction to produce methane and water. Today, synthetic fuel production plants fed by biomass gasification utilize CO methanation at an industrial scale [7].

More recently, CO_2 methanation has attracted the interest of academia and industry as a means of generating fuel from waste CO_2 streams while reducing green house gas emissions. Power to gas systems can utilize the Sabatier reaction as a means of storing excess electrical energy in stable chemical bonds. Methanation reaction conditions such as pressure and temperature are of high relevance to performance. Due to the exothermic nature of these reactions, high temperatures

7

hinder product formation. In contrast, high pressures are shown to increase product formation and conversion [7]. General schematics of CO_2 and CO methanation systems are shown in Figure 2.

(a)   **(b)**
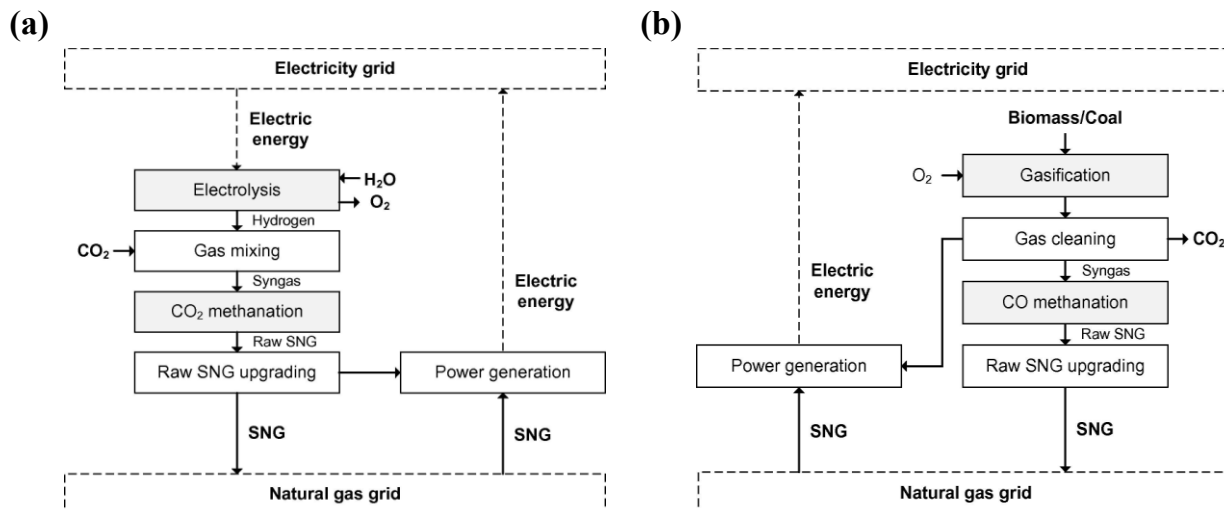
Figure 2. Process schematic of a typical power to gas system for CO_2 methanation (a) and CO methanation (b) [7].

Few pilot and commercial methanation projects have been implemented thus far. Germany heavily focuses on these systems due to their socio-political decision to incorporate large portions of renewable sources into their energy sector. This has lead to an increased demand in energy storage technologies.

In 2009, a pilot plant including a portable methanation reactor was implemented in Stuttgart, Germany with capacity at 25 kW. The system was operated at various locations across Germany and Switzerland from 2009 to 2014 [7]. A larger test plant was built in in Stuttgart in 2012 with a 250 kW capacity using similar technology. Hydrogen gas in all systems was provided via water electrolysis. Etogas Company provided the methanation system consisting of either tube reactors with gas recycling or steam cooled plate reactors [7]. In 2013, a commercial PtG methanation

system was established in Werlte, Germany with a 6300 kW capacity, through collaboration between various energy industries [7]. The technology for the commercial system was provided by MAN.

2.3.   *Power-to-Gas System Configurations*

Power-to-gas systems convert electrical power to chemical bond energy to enable easy storage and deployment of the energy at a different time [5]. There are three major pathways for PtG technology: power to hydrogen, power to SNG and power to renewable content in petroleum fuels. A schematic of the power to gas pathways is shown in Figure 3. Increased investment in volatile renewable energies is bound to create periods of surplus electricity [8]. Adequate energy storage systems must be established to maintain efficiency and sustain the growing renewable market. Current technologies for grid storage include compressed air systems, redox flow batteries, and pumped hydro storage [9]. These technologies are limited by storage time, discharge time and geography [10]. Amongst storage technologies, PtG has shown extensive promise for long-term energy storage. As a result, PtG technologies have been widely researched as a solution for intermittent renewable energy storage [11-14].

The particular configurations utilized by methanation systems is comprised of two distinct steps. In the first step, electrochemical water electrolysis produces H_2 and O_2 gases. Energy must be provided for electrolysis to break the intramolecular bonds of the stable water molecule. The second step utilizes a carbon source to convert CO_2 to CH_4 producing heat and water as by-products. Due to an availability of pre-existing natural gas networks, product SNG can utilize this infrastructure for distribution and storage.
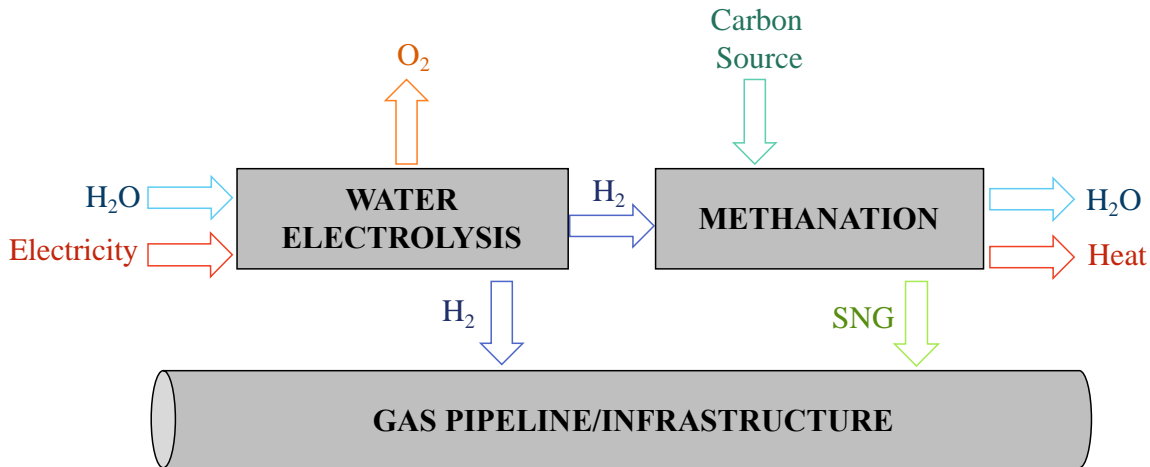
Figure 3. Power to gas system schematic for methanation.

2.4.   *Carbon Feed*

Various carbon sources can be utilized as feed to the PtG system. One option is CO_2 from industrial carbon sources (steel, iron, cement production). Though abundant, this source requires capture and upgrading upstream of the reactor. Another option is biogas which is mainly composed of CH_4 (50-70%) and CO_2 (30-50%) with trace amounts of other chemicals [8]. Biogas is produced from decomposing organic matter in an anaerobic digester. Resultant gas is generally collected and flared to avoid release of CH_4 into the atmosphere, which leads to a wasted energy opportunity. CO_2 emissions from biogas are considered biogenic and therefore do not contribute to industrial green house gas emissions. As a result, biogas processing technologies have gained interest in recent years.

There are three main approaches when dealing with biogas processing. The first involves separation of CH_4 and CO_2 via pressure swing adsorption, amine scrubbing, or membrane technologies. Product CH_4 is then used for heating or injected into natural gas infrastructure while CO_2 is vented to atmosphere [4]. One drawback of this technology is the high cost associated with

the separation processes. The reported cost for this approach is 10-15$/GJ as provided by our industrial partners (Walker Environmental and Integrated Gas Recovery Services - IGRS Ontario, Canada).

A second approach involves electricity generation from raw biogas. Biogas is fed to a combustion unit, which is comprised of an engine, generator and optional cogeneration unit. Much like internal combustion engines, the overall efficiency of such system falls between 35% and 40% with the majority of energy converted to heat. As a result, electricity generation falls short of attractive as an avenue [4].

Lastly, the Sabatier reaction can be utilized to convert residual CO_2 to CH_4 in order to obtain a pipeline quality natural gas stream. Conversion of CO_2 to fuels and chemical helps create an artificial carbon cycle where the otherwise emitted gas is recycled into the energy sector [4]. Though the CO_2 is eventually released to atmosphere, less fossil natural gas would be required with the presence of a renewable component in the natural gas grid. Additionally, the CO_2 emitted is not fossil based but rather from organic matter.

2.5. *Water Electrolysis*

Water electrolysis in an electrochemical cell provides the means for H_2 production. The negatively charges cathode provides the site for chemical reduction as seen by Eq.5. Simultaneous oxidation occurs at the positively charged anode as shown by Eq.6.

$$H_2O + 2e^- \longrightarrow H_2 + O^{2-} \tag{5}$$

$$O^{2-} \longrightarrow \frac{1}{2}O_2 + 2e^- \tag{6}$$

Three current electrolysis technologies include alkaline electrolysis (AEL), polymer electrolyte membranes (PEM), and solid oxide electrolysis (SOEC) [5].

AEL electrolysers use an aqueous alkaline solution (most commonly KOH or NaOH) as electrolyte. This technology is available commercially with units rated up to 2.7 MW. Typical systems operate between 40 ⁰C to 90 ⁰C and show advantageous in the current markets with lower capital costs and large capacities [5]. Disadvantages include low current densities and high maintenance costs associated with the corrosive nature of the electrolyte. Additionally, AEL electrolysers are not ideal for transient operation with cold start times ranging from minutes to hours. Lifetime of AEL electrolysers is reported as approximately 30 years with stack replacement required every 8 to 12 years [5].

PEM electrolysers present a newer alternative to AEL, using solid polymer membranes instead of an alkaline electrolyte [5]. Resulting systems are non-corrosive and benefit from higher power densities and faster cold start times. Commercial systems up to 1.6 MW are available with operating temperatures ranging from 20 ⁰C to 100 ⁰C [5]. However, PEM systems suffer from shorter life expectancies and high capital costs associated with the membrane. This technology is currently more expensive compared with AEL [5].

SOEC electrolysers are the most recent electrolysis technology and are currently being studied at a pilot scale. These units utilize ZrO_2 doped with Y_2O_3 as electrolyte due to the compound's high conductivity to oxygen ions and stability [5]. High temperatures of 800 ⁰C to 1000 ⁰C are required by the system hindering its implementation as a commercial technology. However, these systems show great potential in providing high efficiency electrolysis [5].

2.6. *Catalyst Selection*

A critical requirement for technical feasibility of the methanation system is a highly active and selective catalyst. Heterogeneous catalysts are conventionally composed of metallic nanoparticles dispersed on ceramic supports. It is accepted that reactants first adsorb and dissociate on the catalytic surface. The reaction takes place following this step and products are formed on the catalytic surface. Finally, the products desorb from the surface and exit the reactor [4]. Industrial processes for water gas shift, CO methanation and steam reforming rely heavily on heterogeneous catalysis [4]. Current commercial catalysts for these reactions are manufactured from low cost transitional metals such as Ni, Cu, Cr and Fe. Platinum group catalysts show greater activity but are quite expensive for industrial applications [4].

In General, group 8 to 10 elements from the periodic table can be used as catalysts for the Sabatier reaction. The activity of these metal groups orders as follows: Ru > Fe > Ni > Co > Mo and the selectivity orders as follows: Ni > Co > Fe > Ru [15]. Ruthenium is known to have the highest activity for the Sabatier reaction. However, its high price point compared to Nickel and other commercial catalysts hinders its use in large scale applications [15]. Nickel is the most selective catalyst for the Sabatier reaction and dominates the CO methanation market as the most common commercial catalyst [3]. Highly active and relatively inexpensive, Nickel based catalysts show promising for synthetic natural gas production. One drawback of these catalysts is their high affinity to deactivation by coking [7].

Cobalt based catalysts show similar performance to Nickel catalysts with higher associated costs. For this reason, cobalt catalysts are not used commercially [7]. Iron catalysts exhibit high conversion rates but are known to have low selectivity for CH_4. As a result, these catalysts are

mainly selected for ammonia synthesis or Fischer-Tropsh processes [7]. Molybdenum catalysts have the lowest activity and show greater selectivity for C2+ hydrocarbon. However, they are notorious for having high sulfur tolerances [7]. These catalysts may be beneficial in systems without access to desulfurization treatments.

Aside from active metal selection, supports, promoters and preparation conditions can also affect catalytic activity [7]. Common support materials for the Sabatier reactions include high surface area metal oxides including alumina (Al_2O_3), silica (SiO_2), and titania (TiO_2) with the most common support being alumina with a gamma modification [3].

The activity and stability of all heterogeneous catalysts not based on noble metals is limited by deactivation. Catalysts may experience deactivation by poisoning [16], sintering [17] or coking at high temperatures [18]. The presence of sulphur compounds such as H_2S in the feed gas causes poisoning of the catalyst. Poisoning represents the loss of catalyst activity due to the strong chemisorption of sulphur to active sites [19]. Deactivation from poisoning is irreversible and quick in the absence of upstream desulphurization processes and eventually leads to complete loss of activity in the catalyst [4].

Sintering results at high temperatures from nanoparticle migration leading to growth of larger nanoparticles to reduce surface energy. This phenomenon leads to loss of active surface area causing catalyst deactivation. With sintering, deactivation rates slow with time and full deactivation is never achieved [4]. For Nickel based catalysts, sintering presents in the form of $Ni(CO)_4$ on the active surface [17]. Sintering can be controlled by operating the reactor at moderate temperatures.

Coking represents the deposition of carbon on the catalytic surface leading to deactivation though surface fouling, blocked pores and disintegrated support [20]. Three dominant pathways

for coking include the Boudouard reaction (Eq.7), CO reduction (Eq.8) and CH4 cracking (Eq.9). The Boudouard reaction and CO reduction dominate at low temperatures while CH4 cracking is predominately seen at high temperatures and low CO partial pressures [4].

$$2CO \leftrightarrow C + CO_2 \tag{7}$$

$$CH_4 \leftrightarrow C + 2H_2 \tag{8}$$

$$CO + H_2 \leftrightarrow C + H_2O \tag{9}$$

Heat removal is key to controlling catalyst deactivation by sintering and coking. Temperatures should be kept below 800 K for optimal reaction conditions. Additional upstream desulphurization is also required to protect the catalyst against poisoning. Nickel based catalysts are widely used in industrial applications due to their excellent activity, high selectivity and low cost. One study assessed catalytic performance of commercial Nickle-based catalyst both numerically and experimentally and found CO2 conversion as high as 90-95% and complete selectivity to CH4 at elevated pressures and moderate space velocities [21]. Additionally, no deactivation was observed during 100 h TOS [21].

2.7. Reactor Design

Of equal importance is development of a reactor configuration, which can support the unique challenges associated with methanation. Common reactor design for heterogeneous thermocatalytic reactions is fixed bed and fluidized bed. Among advantages of fixed beds are their compact size and simplicity. However, these reactors show problematic in heat management when encountering a highly exothermic system. This results as heat transfer in packed beds is inefficient [4]. Typical operating ranges for methanation reactor are between 200 °C and 550 °C and 1 to 100

bar [5]. The highly exothermic nature of the Sabatier reaction leads to hotspot formation which results in catalyst deactivation, mechanical disintegration and inhibits product formation [22]. One solution is use of a cascade of adiabatic reactors with intermediate cooling and gas recirculation. Many different configurations for such a system have been suggested in literature. Although a great level of control can be achieved with a cascade of adiabatic reactors, the substantial increase in required equipment leads to process complexity and increased capital and operating costs [7]. A schematic of a cascade of adiabatic reactors is shown in Figure 4.
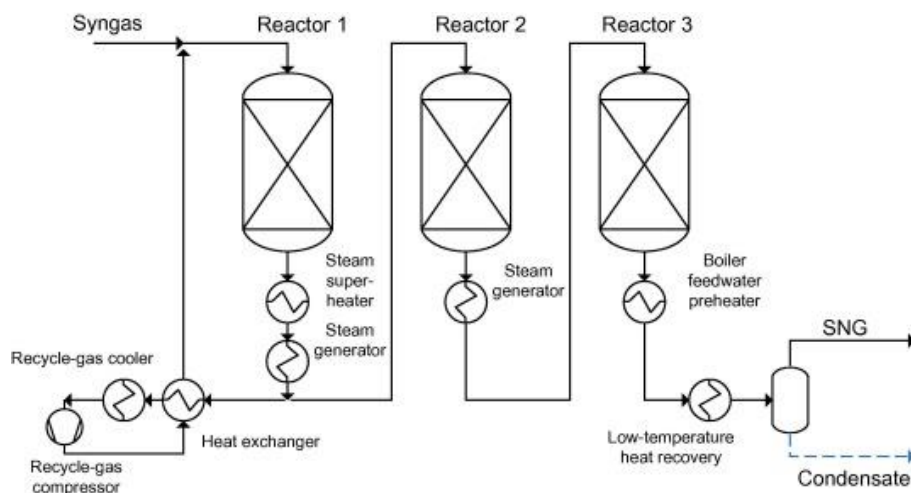
Figure 4. Conceptual schematic of a cascade of adiabatic reactors with intermediate cooling and gas recirculation [7].

Alternatively, single pass and actively cooled reactors can be used to optimize heat removal and avoid hotspot formation. Such configurations require simple process controls and fewer equipment. However, the complicated structure of the reactor lends to high capital requirements, non-trivial methods of catalyst deposition and replacement, and expensive operating costs [4]. Despite these challenges, many single pass reactor configurations have been studied in literature including structured microchannel reactors [23] and monolith reactors [24-26]. Alternative to fixed

bed reactors, fluidized beds have been studied extensively and shown to exhibit excellent heat transfer characteristics [27, 28]. A single pass fluidized bed can therefore be utilized in the Sabatier system lowering process control requirements. Disadvantages of fluidized beds include bulky appearance, catalyst attrition and narrow range operation dictated by fluidization velocity [4]. Three phase slurry reactors have shown promise in providing nearly isothermal reaction conditions [29, 30]. However, the unique limitations associated with these reactors include a narrow operating window dictated by solvent/heat transfer fluid properties and mass transfer between gas and liquid [7]. An actively cooled heat exchanger type packed bed reactor provides a low cost solution for near isothermal operation. Process optimization is required to determine the heat transfer fluid rate that provides sufficient heat removal while keeping the process optimized.

2.8. *Techno-economic Assessment*

A technically feasible Power-to-Gas (PtG) system for SNG production must incorporate Sabatier reactors and electrolysers with auxiliary process units that provide the necessary conditions for optimal operation. Few techno-economic studies have focused on the methanation of pure CO_2 streams into SNG [6, 9]. One study evaluated the feasibility of a system which combined alkaline electrolysis and chemical methanation with a post combustion CO_2 feedstock [9]. Revenue sources were identified as the product SNG and O_2 gas produced via electrolysis. Results showed the cost of SNG to be lowest in Ontario, Canada at 70 EUR/MWh and highest in Spain at 125 EUR/MWh with all commodity prices based on local rate [9]. A different study focused on a pure CO_2 feed combined with a membrane reactor and PEM electrolyser and evaluated the profitability of the system as a function of production factors including electricity

price and loading period [6]. Their findings indicated that the profitability of the project is highly dependent on low electricity prices and higher loadings [6].

Practical realization of the CO_2 methanation technology requires selection of an appropriate CO_2-rich feedstock. An excellent source for this feedstock is biogas, which is primary composed of CH_4, which is the target product. Unlike post combustion CO_2, however, biogas contains trace amounts of unwanted gases which must be removed either upstream of the process to ensure optimal operation or prior to pipeline injection to meet pipeline specifications. Various groups in academia and industry have tackled the techno-economics of SNG production via biogas.

A study proposed economics for a 60 SCFM (1.34 MW power rating) plant with feed biogas derived from dairy manure [31]. It was found that the capital investment and annual operating costs would be approximately $5,194,000 CAD and $693,377 CAD respectively [31]. Assuming the SNG selling price of $40/GJ (due to environmental incentives), it was found that the process would be feasible with a payout period of 4.5 years [31]. A different group focused on 125 SCFM feed from anaerobic digestion of sewage sludge and compared various upgrading and PtG technologies against one another. Direct methanation showed an annual production cost of €1,650,000 [8]. It was also found that that direct methanation of biogas showed higher feasibility under continuous rather than intermittent operations. Comparisons between systems with methanation of raw biogas with those separating CH_4 and CO_2 prior to methanation have also been made [31, 32]. It was found that there was negligible differences between the two in terms of reactor performance with the former option showing desirable economics [8]. Figure 5 provides the process flow diagrams for the abovementioned systems.
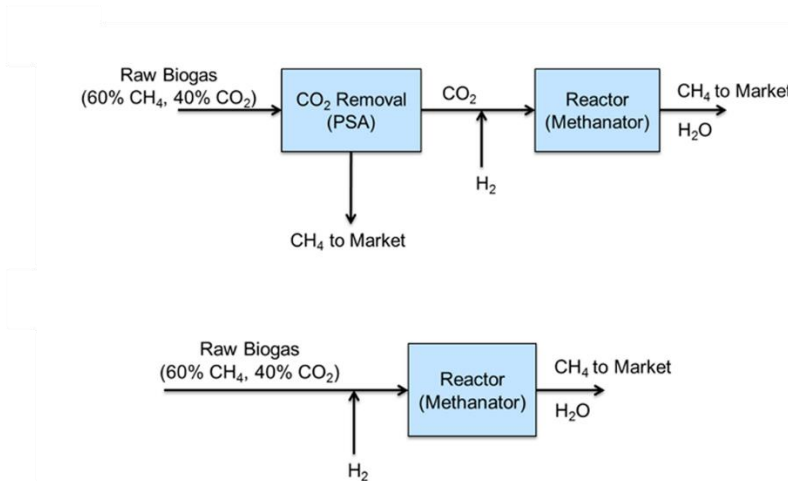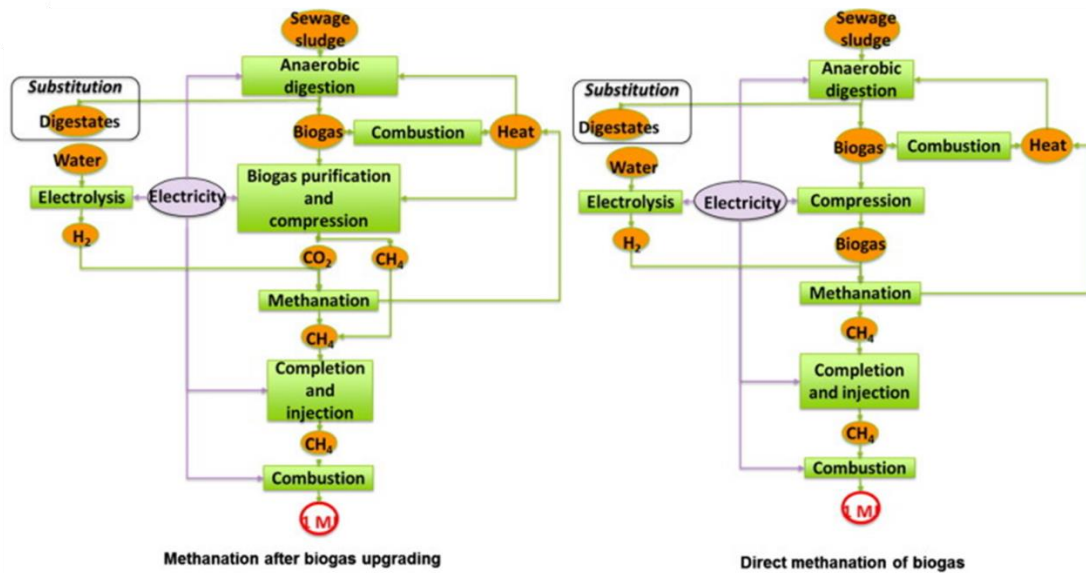
Figure 5. Process flow diagram of methanation systems from a 60 SCFM biogas plant from manure [31] (upper panel) and a 125 SCFM biogas plant from sewage sludge [8] (lower panel)

3. Methods

3.1. *Reactor Model*

3.1.1. *Reactor Configuration*

A schematic representation of the suggested actively cooled Sabatier reactor is shown in Figure 6. The reactor consist of a heat-exchanger type configuration comprised of two compartments. The packed bed reaction compartment is internally cooled by the coolant of choice flowing in multiple tubes. Reactor dimensions are listed in Table 1.
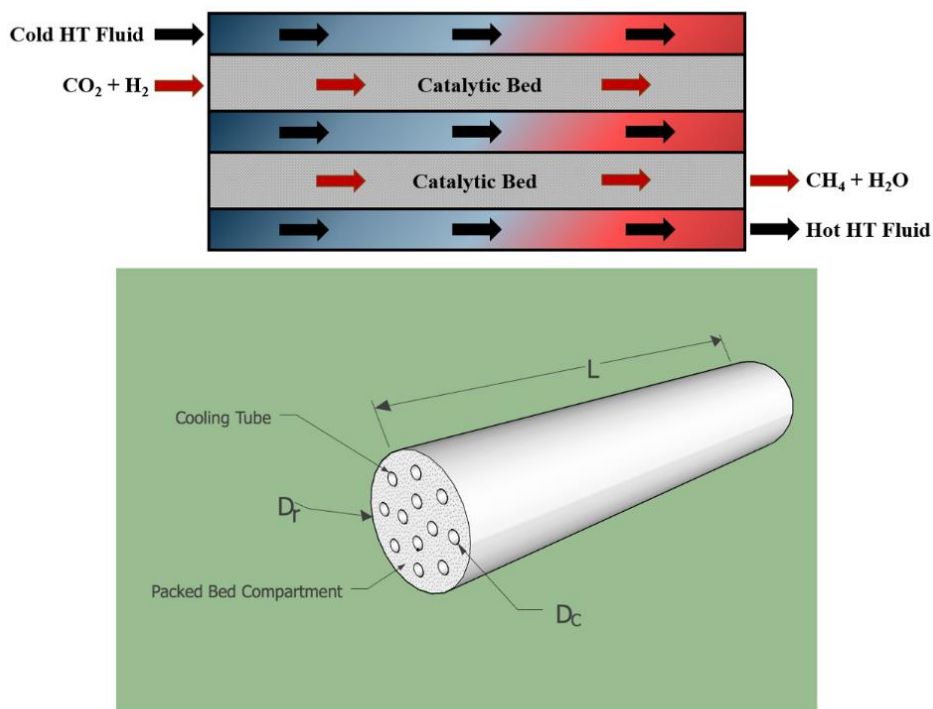
Figure 6. Actively cooled, packed bed Sabatier reactor showing a conceptual schematic (upper figure) and multi-tube, heat exchanger-type configuration (bottom figure).

For a biogas feedstock, the feed mixture contains CH_4, CO_2 ($CH_4/CO_2 = 1.44$), and N_2, while keeping identical H_2/CO_2 ratio ($H_2/CO_2 = 4$). It is assumed that the biogas only contains CH_4, CO_2, and N_2, with all impurities being removed upstream (more details provided in section 3.1.2). All simulation parameters are listed in Table 1. All symbols and abbreviations listed in Nomenclature. Space velocity is defined as follows per Eq.10.

$$SV = \frac{\varepsilon v_{gf}}{L} \tag{10}$$

The reference coolant gravimetric flow rate is defined when the heat generation rate is equal to the rate of heat removal by the coolant (assuming that $\Delta T_c = 300$ K) and shown by Eq.11 [22, 33].

$$G_{c,0} = \frac{y_{CO_2} \Delta H_{SR} F_{tf}}{C_{pc} \Delta T_c} \qquad\qquad F_{tf} = \rho_{gf} V_{PB}\, SV \tag{11}$$

Table 1. Reactor dimensions and operating parameters.

Parameter	Symbol	Value	Unit
Packed bed compartment diameter	D_r	0.3	m
Reactor length	L	1.5	m
Coolant tube diameter	D_c	0.05	m
Number of cooling tubes	N_c	12	-
Reactor and cooling tube wall thickness	d_w	0.002	m
Insulation layer thickness	d_{iw}	0.05	m
Catalyst pellet diameter	d_p	0.005	m
Hydrogenation (H_2/CO_2) ratio	H_2/CO_2	4	-
Biogas composition (CH_4/CO_2) ratio	CH_4/CO_2	1.44	-
Reaction compartment outlet pressure	$P_{t,out}$	10	bar
Coolant (compressed air) pressure	P_c	10	bar
Reaction compartment feed temperature	T_f	550-650	K
Coolant feed temperature	$T_{c,f}$	550-650	K
Packed bed space velocity	SV	750	h^{-1}
Normalized cooling rate	$G_c/G_{c,0}$	0.1-10	-

3.1.2.   *Model Formulation*

A transient, 1D, pseudo-homogenous model [22, 33] was used to simulate the reactor. The model does not account for radial gradients, but 1D models normally describe well relatively small packed beds, at least capturing qualitative trends [34]. The reactor geometry was configured to minimize the radial distance between the compartments to justify the 1D approximation.[22, 33] Unlike previous modelling studies, the model accounts for temperature variations in the coolant tubes rather than assuming constant coolant temperature. The model also includes axial mass and heat dispersion and the temperature dependence of thermo-physical properties. Including axial

heat dispersion is of particular importance because it can lead to non-trivial effects, such as upstream moving thermal fronts.[22, 33, 35, 36] Ideal gas behavior was assumed.

Component mass balances for the packed bed are given by Eq.12 ($i \equiv H_2$, CO_2, CO, CH_4, H_2O; $j \equiv 1, 2, 3$). Energy balances in the packed bed and coolant compartments are described by Eq.13 and Eq.14. Initial and boundary conditions are listed in Eq.15 and Eq.16. Reaction kinetics and kinetic and transport parameters are given in Appendices A-C; notation is explained in Nomenclature.

$$\varepsilon \frac{\partial C_i}{\partial t} = D_{ae} \frac{\partial^2 C_i}{\partial z^2} - \varepsilon^k \frac{\partial(v_g C_i)}{\partial z} + (1-\varepsilon)\rho_s \sum_j \eta_j \alpha_{ij} R_j \tag{12}$$

$$(\varepsilon \rho_g C_{pg} + (1-\varepsilon)\rho_s C_{ps}) \frac{\partial T}{\partial t} = k_{ae} \frac{\partial^2 T}{\partial z^2} - \varepsilon \rho_g C_{pg} v_g \frac{\partial T}{\partial z} +$$
$$+ (1-\varepsilon)\rho_s \sum_j (-\Delta H_j)\eta_j R_j - U_{w,HE} a_{r,HE}(T - T_c) - U_{w,HL} a_{r,HL}(T - T_e) \tag{13}$$

$$\rho_c C_{pc} \frac{\partial T_c}{\partial t} = \lambda_c \frac{\partial^2 T_c}{\partial z^2} - \rho_c C_{pc} v_c \frac{\partial T_c}{\partial z} - U_{w,HE} a_{c,HE}(T_c - T) \tag{14}$$

$$z = 0 \qquad (\varepsilon v_{gf})^k (C_{i,f}^k - C_i^k) = -D_{ae}^k \frac{\partial C_i^k}{\partial z} \qquad\qquad z = L \qquad \frac{\partial C_i^k}{\partial z} = 0$$

$$\varepsilon \rho_g v_{gf} C_{pg}(T_f - T) = -k_{ae} \frac{\partial T}{\partial z} \qquad\qquad\qquad \frac{\partial T}{\partial z} = 0 \tag{15}$$

$$\rho_c v_c C_c(T_{c,f} - T_c) = -\lambda_c \frac{\partial T_c}{\partial z} \qquad\qquad\qquad \frac{\partial T_c}{\partial z} = 0$$

$$t = 0 \qquad C_i^k(0, z) = C_{i,\text{int}}^k$$
$$T(0, z) = T_{\text{int}}$$
$$T_c(0, z) = T_{c,\text{int}}$$
$$a(0, z) = 1 \tag{16}$$
$$c(0, z) = 0$$

The change in the gas velocity due to the change in number of moles in the reaction was calculated using Eq.17 as follows.

$$v_g = \frac{v_{gf}}{C_{tf}} \sum_i C_i \tag{17}$$

Pressure drop was accounted for using the Ergun equation shown by Eq.18 (in a practical situation will be set by a back pressure regulator).

$$\frac{dP_t}{dz} = -150 \frac{(1-\varepsilon)^2 \mu_g}{d_p^2 \varepsilon^3} v_g - 1.75 \frac{(1-\varepsilon)\rho_g}{d_p \varepsilon^3} v_g^2 \tag{18}$$

3.1.3.   Numerical Simulation

The model was solved using the MATLAB PDE solver with a second order accurate spatial discretization based on a fixed set of user-specified nodes and time integration done by the stiff ODE solver (ode 15s). Dependences of thermo-physical properties (density, viscosity, gas diffusivity, heat capacity and thermal conductivity) on temperature, pressure and composition were accounted for using polynomial regressions fitted to the data on thermo-physical properties from the literature [37-40]. Void fraction (ε) was set to 0.5.

3.2.   Process Model

3.2.1.   Model Formulation

Biogas primarily consists of CH_4, CO_2, N_2, and O_2 gases. Trace amounts of H_2S, NH_3, siloxanes (Si), volatile organic compounds (VOC) and water vapor can be present in biogas in compositions unique to the emission source. Landfill gas is produced via the anaerobic breakdown

of waste by microorganisms, providing the source of biogas for this study. Commonly reported compositions for LFG are 50%-80% CH_4, 20%-50% CO_2, 0%-5% N_2, and 0%-1% O_2, with trace amounts of H_2S, siloxanes (Si), volatile organic compounds (VOC) and water vapor [41]. For this study, LFG compositions were cordially provided by our industrial partners (Walker Environmental and Integrated Gas Recovery Services - IGRS Ontario, Canada) as presented in Table 2. Additional system requirements include water supplied for electrolysis to provide a 4:1 ratio of H_2 to CO_2 and electricity from the grid to meet the power demands.

Table 2. Typical Landfill gas feed specifications.

Parameter	Value
$y(CH_4)$	42% vo.02l.
$y(CO_2)$	29% vol.
$y(N_2)$	23% vol.
$y(O_2)$	4% vol.
$y(H_2O)$	2% vol
$y(Si)$	60 ppm
$y(H_2S)$	600 ppm
$y(VOC)$	3000 ppm
Temperature	35 °C
Pressure	2.7 bar
Flowrate	5000 scfm

For injection to an existing conventional natural gas pipeline, the product SNG must meet pre-defined gas specifications. This study uses pipeline quality specifications based on the Canadian mainline pipeline as shown in Table 3 to examine compliance for product quality [42]. Delivery pressure of the SNG to pipeline must be within the 100-400 psig range.

Table 3. Pipeline Gas Quality Specifications for Natural Gas [42]

Spec	Requirement
CO_2	< 2% vol.
O_2	< 0.4% vol.
N_2	< 4% vol.
H_2S	< 23 mg/m^3
Total Sulfur	< 115 mg/m^3
H_2O	< 65 mg/m^3
Temperature	< 50 °C
Dew Point	Max: -10 °C (at 5500 kPa absolute)
Heating Value	Min: 36 MJ/m^3 Max: 41.34 MJ/m^3

The system designed in this study address all abovementioned challenges. An overview of the resulting system is shown in Figure 7 through four interacting subsystems:

(1). Biogas Conditioning

(2). Hydrogen Generation

(3). Methanation

(4). Product Upgrading
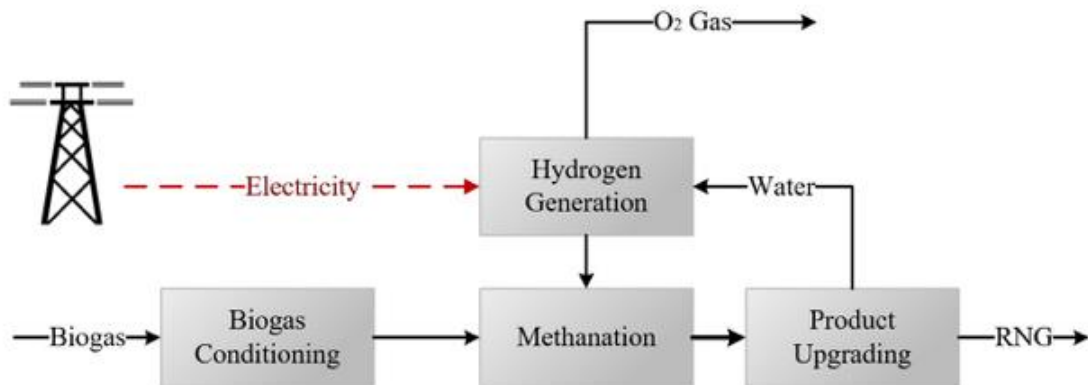
Figure 7. SNG production system block flow diagram

3.2.2. Steady State Model

Chemical process simulation software Aspen HYSYS was used to construct a steady state mathematical model of the system. Rigorous calculations and iterations were performed to solve unit operations and provide design details for each piece of equipment. Simultaneous heat and material balance calculations over the whole system allow specification of all process stream. HYSYS inherently uses a fluid package to calculate thermodynamic properties and phase equilibria. Peng Robinson was the chosen as the fluid package of choice due to high sophistication, affinity to hydrocarbon processes and high range for process conditions. The process model provided an overview on process and utility requirements for continuous operation. Additional features in HYSYS allowed detailed equipment design and modelling. Details for this are provided per unit type in the following sections.

3.2.3. Electrolysers

Electrolysers are modelled in Aspen HYSYS as conversion reactors. Kinetics are controlled by a conversion value set by the user. Product specification is determined by the conversion value. Large H_2 demands of the 5000 SCFM methanation system require simultaneous operation of multiple electrolysers. Specifics of electrolyser design are not included in the process simulation but obtained from online information on commercial units. Data on large scale electrolysis systems provided by Nel hydrogen [43] is utilized to determine the utility requirements, efficiency and capital cost of the electrolysers in this project.

3.2.4. Heat Exchangers

Heat exchanger in HYSYS were solved through integrated material and energy balance equations for the cold and hot fluids. All process conditions were specified for both the inlet process fluid and heat exchange fluid [44]. In order to satisfy all degrees of freedom, the outlet temperature of either heat exchange fluid or process fluid was also specified. A simple end point model was initially utilized to calculate temperatures, pressure, heat flow and UA in the exchangers. A mathematical representation of this model is provided by Eq.19 and Eq.20 where the balance error equated to zero due to the steady state operation [44]. For this study, it was assumed that no duty is lost or gained due to heat loss or heat leak.

$$Balance\ Error = (M_{cold}[H_{out} - H_{in}]_{cold} - Q_{leak}) - (M_{hot}[H_{out} - H_{in}]_{hot} - Q_{loss}) \quad (19)$$

$$Q = UA\Delta T_{LMTD}F_t \quad (20)$$

Aspen Exchanger Design and Rating program (EDR) using the standard method was subsequently used to perform advanced exchanger sizing and error checking. Process fluids were allocated to prefer heavier fouling streams on tube side. Aspen EDR allowed for design and optimization of exchanger details including TEMA type, exchanger orientation, tube and shell size, tube and shell passes, baffle number and orientation and pitch size and orientation [44]. Additionally, pressure drops though both shell and tube side were identified by EDR.

3.2.5. Pumps

HYSYS utilizes steady state hydraulic calculations to determine the duty of each pump with the general assumption that the liquid is incompressible [44]. Suction stream conditions are fully specified for the model as well as the differential pressure desired. Eq.21 provides the

mathematical model used by the software to determine the ideal pump duty. With inherent losses due to efficiency, the actual pump duty is calculated by using Eq.22 [44]. For the purpose of this study, the pump efficiency was set to a common industry reported value of 75%. It should be noted that any excess energy not utilized by the pump motor for mechanical work directly contributed to raising the temperature of the discharge stream proportionally.

$$Power\ Required_{ideal} = \frac{(P_{out} - P_{in}) \times F_{liquid}}{\rho_{liquid}} \tag{21}$$

$$Efficiency\ (\%) = \frac{Power\ Required_{ideal}}{Power\ Required_{actual}} \tag{22}$$

3.2.6. Reactors

HYSYS obtains packed bed reactor (PBR) profiles by dividing the reactor into several sub volumes and solving the steady state mole balance, given in Eq.23. The reaction rate is considered to be spatially uniform within each sub volume. Radial gradients and axial mixing are assumed to be negligible.

$$F_{j0} - F_j + \rho_s \frac{(1-\varepsilon)}{\varepsilon} \int_V r_j' dV = 0 \tag{23}$$

The same reaction rates expressions used in the MATLAB model can be implemented in the HYSYS model. Pressure drop within the PBR is calculated using the Ergun equation, Eq.18. The duty of each PBR sub volume is rigorously calculated using local heat transfer coefficients for both the PBR, and the utility fluid, given in Eq.24 and Eq.25 respectively.

$$Q_j = U_j A(T_{PBR,j} - T_{util,j}) \tag{24}$$

$$Q_j = m\rho C_p(T_{util,j} - T_{util,j+1}) \tag{25}$$

Local heat transfer coefficients inside the PBR tube can be inputted by the user, calculated empirically or calculated from the Nusselt number using standard correlations.

3.2.7.   Compressors

Theoretical principles for compressor design in HYSYS rely on thermodynamics of mechanical work on a reversible process as shown in Eq. 26 [44]. Inputs require a fully specified inlet stream, desired outlet pressure and compressor efficiency. Adiabatic centrifugal compression is calculated through isentropic lines connected from inlet to outlet conditions [44]. Actual power requirements for the unit can be determined from Eq.27. Using the ideal outlet enthalpy, pressure and efficiency, HYSYS calculates the actual outlet enthalpy and subsequently the outlet temperature [44]. Similar to pumps, the compressor efficiency was set to a common industry reported value of 75%.

$$W = \int VdP \tag{26}$$

$$Efficiency\ (\%) = \frac{Power\ Required_{isentropic}}{Power\ Required_{actual}} \tag{27}$$

3.2.8.   Separators

Separation vessels in HYSYS are modelled in steady state conditions based on a P-H flash [44]. The resultant thermodynamic model determines product compositions and phases. Vessel operating pressure is set to the inlet pressure with the pressure drop through the vessel assumed

negligible. Conditions of vapour liquid equilibrium are achieved through preheaters upstream of the separators. Equilibrium parameters are calculated based on the selected fluid package [44].

3.3.   *Economic Model*

Technical design parameters output by the HYSYS steady state model were fed to Aspen economics where the base modular cost (BMC) of the units was determined. This value included both the cost of the standalone unit and the cost of installation. Capital cost estimates for dynamic units including adsorption columns were obtained from our industry partners (Walker Environmental and Integrated Gas Recovery Services - IGRS Ontario, Canada). Utilities requirements mainly consisting of water and electricity were determined through heat and material balances provided by HYSYS. Paired with maintenance and labour costs, these values provided the basis for annual operational costs. A detailed economic model was further used to calculate financial parameters including total capital investments, present worth, net present worth, payout period and internal rate of return. This model is presented in detail in the results section and provides the basis of the feasibility study. Units of cost for all subsequent values are in USD (2018). An exchange rate of $1.3 CAD/USD was used throughout the calculations when necessary.

4. Results and Discussion

4.1.   Methanation Reactor Design

4.1.1.   MATLAB Model

The technical feasibility of the SNG PtG process is dependent on the actively cooled Sabatier reactor achieving high methane yields. Figure 8 shows the performance of a large-scale (67 L) reactor, which could be run in parallel with other reactors in an array.
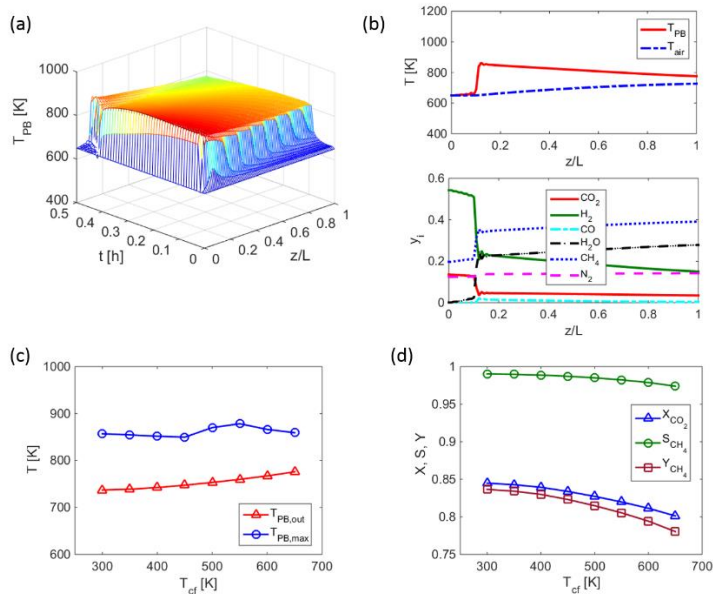
Figure 8. Spatiotemporal profile of packed bed temperature (a), spatial profile of temperature (upper panel) and mole fraction (lower panel) (b), reactor packed bed compartment temperature as a function of inlet cooling fluid temperature (c) and reactor performance as a function of inlet fluid temperature (d). *Parameters:* $P_{t,f} = 10$ bar, $G_c = 0.5\ G_{c,0}$, TOS = 0.5 h, SV = 750 h^{-1}, $T_f = 650K$, $H_2/CO_2 = 4$, $CH_4/CO_2 = 1.44$, $T_{c,f} = 650K$ (upper panels), $D_r = 0.3m$, $D_c = 0.05m$, $L = 1.5m$, $d_p = 0.005m$, $N_c = 12$.

Figure 8a and 8b show that the spatiotemporal temperature profile and spatial temperature and mole fraction profiles of the reactor. The heat transfer between the packed bed and coolant tubes is quite efficient, although there is a significant difference between the bed and coolant temperatures (Figure 8b). Next, the reactor performance is evaluated as a function of the coolant feed temperature (Figure 8c and 8d). Lowering the inlet coolant temperature decreases the reactor outlet temperature significantly, while the maximum bed temperature remains similar (Figure 8a). An important observation is that decreasing the packed bed outlet temperature due to more efficient cooling results in a significant conversion improvement (Figure 8d).

4.1.2. *HYSYS Integration*

To verify that the reactor model simulated in MATLAB can be reproduced in the process simulation software, a packed bed, air-cooled reactor model was defined and simulated in Aspen HYSYS.
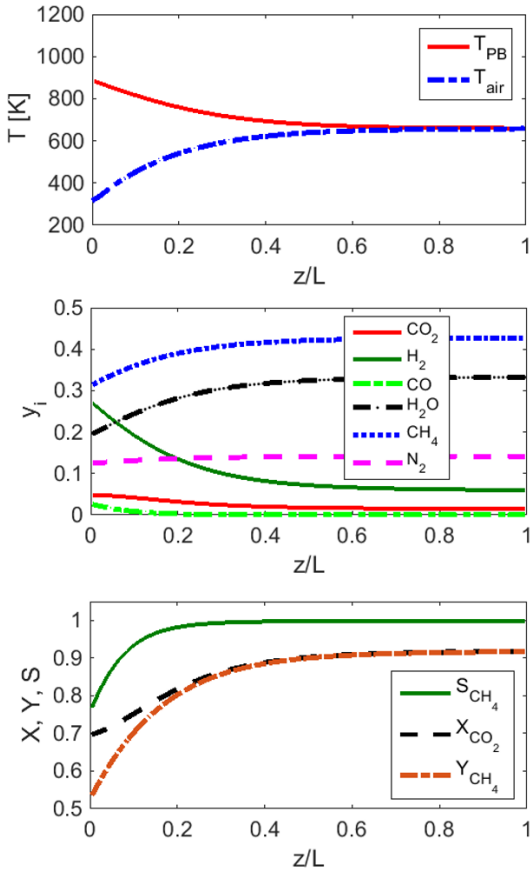
Figure 9. Spatial profiles of temperature (upper panels), mole fractions (middle panel) and reactor performance (lower panel) in the HYSYS-simulated air-cooled packed bed Sabatier reactor. T_{PB} and T_{air} are the temperatures of the packed bed and coolant (air) respectively. *Parameters:* $P_{t,f}$ = 10 bar, $G_c = 0.9G_{c,0}$, SV = 750 h^{-1}, H_2 /CO_2 = 4, CH_4/CO_2 = 1.44, D_r = 0.3 m, L = 1.5 m, d_p = 0.005 m, T_f = 575 K, $T_{c,f}$ = 300 K.

The HYSYS reactor model dimensions were chosen to match the dimensions of the previously examined air-cooled, biogas-fed reactor (Figure 9). The same reaction rate expressions and kinetic parameters used in the MATLAB model were used in the HYSYS model. Pressure drop in the HYSYS model was calculated using the Ergun equation and found to be negligible. Catalyst properties and heat transfer parameters were also taken from the MATLAB model. Figure 9 shows

simulated spatial profiles of the reactor temperature, mole fractions and reactor performance (conversion, selectivity and yield). Examination of these results showed that the HYSYS simulated reactor produced results resembling those simulated in MATLAB. The HYSYS reactor model predicts that the hot spot is located at the reactor entrance and that the outlet streams exit at identical temperatures. This results as the HYSYS model does not account for axial diffusion.

4.2.   System Design

4.2.1.   Biogas Conditioning

The biogas conditioning unit is designed to pre-treat the feed and prepare the reactant biogas to be fed to the methanation reactor. Components such as water vapour, H_2S, Siloxanes, and VOCs can lead to operational failure and must be removed upstream of all process units. The first treatment process removes water to prevent downstream corrosion and hydrate formation. The incoming stream is chilled in a shell and tube heat exchanger (STHE) with ethylene glycol as heat transfer fluid to condense in stream water. The stream is subsequently passed through a water knock out drum where the condensed liquid water exits at the bottom and is stored in the water tank. The dehydrated biogas stream passes through another STHE to super-heat any remaining vapour eliminating the possibility of entrained liquid in the stream.

Biogas then passes through the desulfurization skid. The presence of H_2S in a gas stream poses both environmental and health concerns. This gas is toxic, flammable and notorious for catalyst poisoning and subsequent deactivation. Additionally, H_2S is corrosive to metallic surfaces of pipes, engines, pumps and other process equipment. Entering biogas is sweetened by an activated carbon adsorption tower. Activated carbons show good adsorption capacity for H_2S, are widely available and relatively inexpensive. The unit consists of two towers, which reduces H_2S concentrations to

≤1.5 ppm. Operational and maintenance needs for the unit arise as the media must be replaced every 6-months and disposed appropriately.

Subsequently, the stream is passed through a temperature swing adsorption (TSA) unit for the removal of siloxanes and VOCs. Siloxanes result in equipment wear and fouling when combusted in gas turbines, boilers or combustion engines resulting in the deposition of a powdery silicon dioxide on process surfaces. This can cause increased maintenance, downtime and cost. The TSA unit consist of two pressure vessels filled with a desiccant based media. The incoming stream passes through the active column where siloxanes and VOCs adsorb to the surface of the media. At the same time, the second column is regenerated with heated air. Operational costs for the unit include replacement of the regenerative media every 12-18 months and electricity costs for the ambient air blower and heater. Due to the presence of VOCs in the regenerate air, this stream cannot be released to atmosphere and must be incinerated in an enclosed flare. The final step for the biogas conditioning skid is compressing the biogas stream to approximately 10 bars. This inlet pressure is required for optimal performance of the methanation reactor.
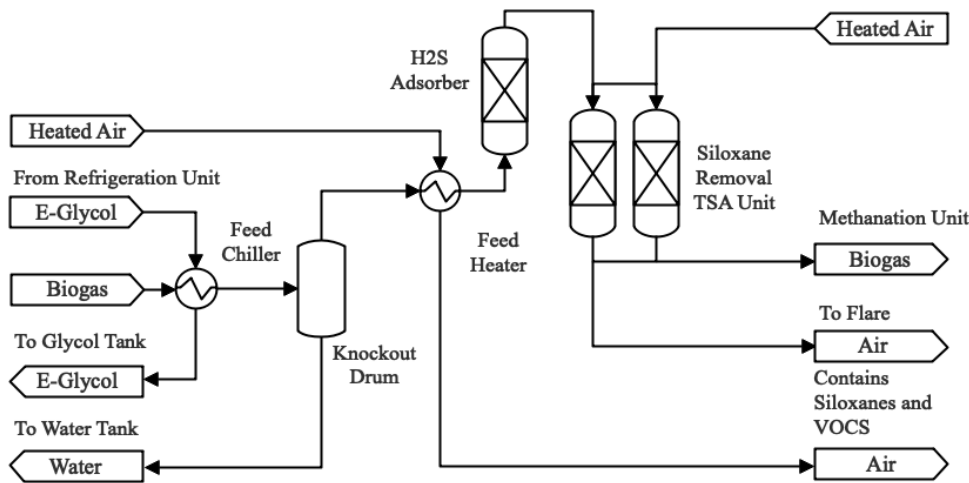
Figure 10. Biogas conditioning unit process flow diagram

4.2.2.　　　*Hydrogen Generation*

Hydrogen production runs simultaneous with the biogas conditioning unit. Water feeds into the alkaline electrolysers where electricity from the grid is utilized and converted to chemical energy via hydrogen and oxygen gas production. Three current electrolysis technologies include alkaline electrolysis (AEL), polymer electrolyte membranes (PEM), and solid oxide electrolysis (SOEC) [5]. Between the options, AEL electrolysers show the greatest promise in the current market [5] . The by-product oxygen gas is vented to atmosphere, as it is not used by the downstream process. Capital costs and utility requirements for the 45 MW electrolysis unitsare based on information published by Nel hydrogen [43]. Operational costs account for electricity and water requirements for the system. Maintenance is required to replace cell stacks every 7 years. Finally, the pure H_2 stream leaving the electrolyser is then compressed to 10 bars to match the biogas stream.
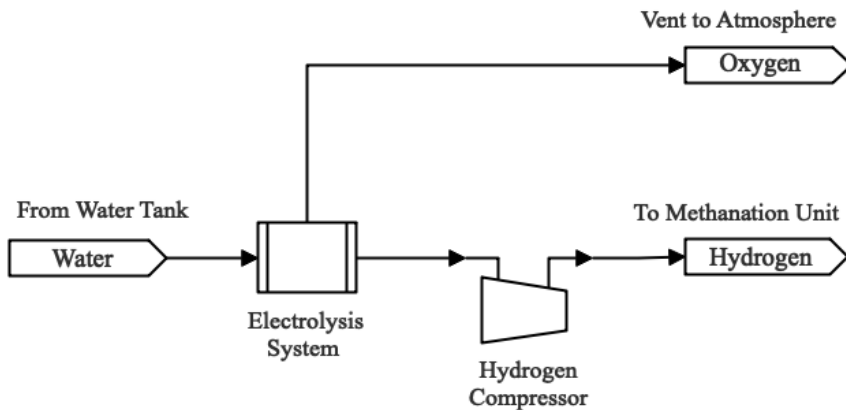
Figure 11. Hydrogen generation unit process flow diagram

4.2.3. Methanation

Compressed H_2 and biogas streams enter the methanation unit simultaneously. Each individual stream enters a STHE through which the gas is superheated to 300 ℃. This temperature is selected for optimal reactor operation. Both streams are then mixed and fed to the methanation system, which consists of large number of packed bed reactors operating in parallel. The highly exothermic Sabatier reaction takes places in the reactors producing product SNG. Additionally, any O_2 present in the biogas stream reacts with H_2 to produce water. Heat released via the reaction must be removed to promote CH_4 production, prevent reactor overheating and protect the catalyst against deactivation. The heat exchanger type reactor utilized in this system makes use of compressed air to actively cool the length of the reactor. Despite active cooling, high temperatures persist in the reactor outlet. To make the process more economical, the reactor outlet is used as heat exchange fluid for the H_2 and biogas preheaters. Maintenance costs for the methanation unit arise from catalyst replacement costs and general maintenance for the heat exchangers.
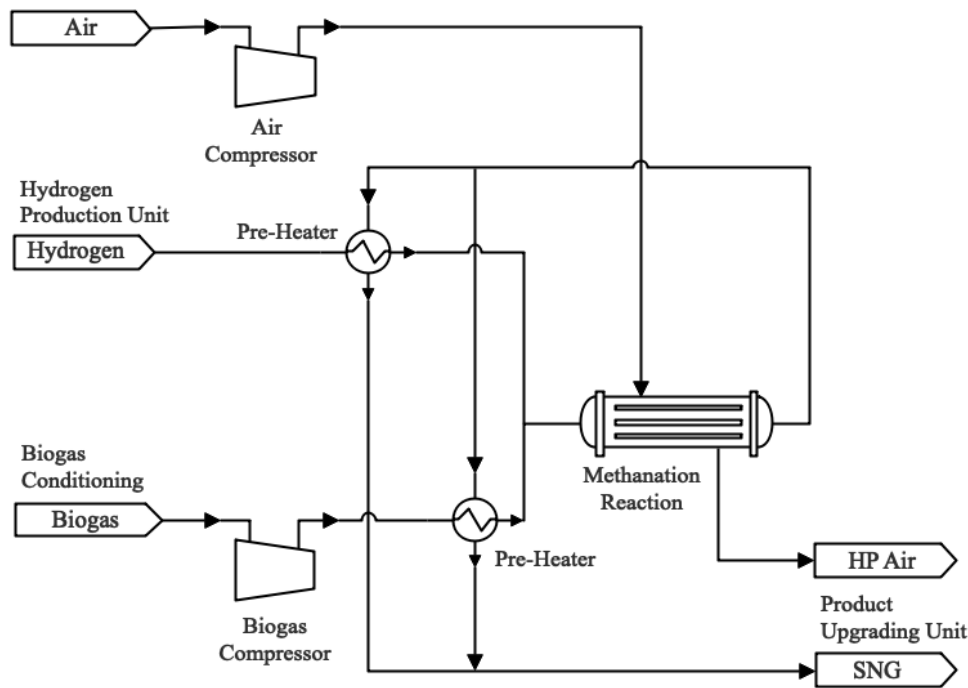
Figure 12. Methanation system process flow diagram

4.2.4. *Product Upgrading*

Following the methanation system, the product gas must go through strict purification to ensure its compliance with pipeline specifications. The product stream contains considerable fractions of water vapour as a result of the Sabatier reaction. The stream is sent though three STHEs in order to condense all water vapour to liquid form. The first STHE utilized compressed air for cooling medium while the second and third make use of ethylene glycol. The selection of heat exchange medium results from the differential temperatures required by each exchanger. Once the fluid has passed though the cooling exchanger train, it enters the water knockout drum. Liquid water exits the bottom and is stored in the water tank. There is significant amount of water produced in this step, which is later used as partial feed to the electrolyser. This allows for resource recycling and helps the economics of the system. The final step of the system consists of a pressure swing

adsorption (PSA) unit that utilizes carbon molecular sieve to separate N_2 from the product gas. The presence of an inert gas in SNG lowers the heating value when compared to conventional natural gas. The removal of this gas is important to meet the Wobbe Index specification for the product SNG. Major operational cost contributions to the PSA unit are from electricity requirements for creating the pressure differentials. Following the PSA, the product stream is suitable in composition for pipeline injection.
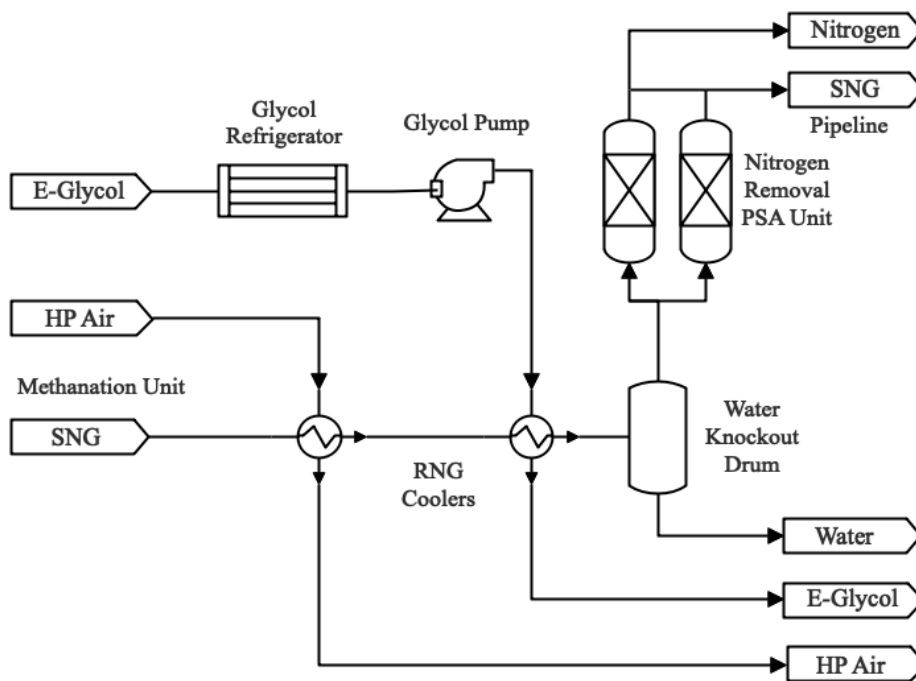
Figure 13. Product upgrading unit process flow diagram.

4.3.   Economics

A complete process simulation of the abovementioned process was constructed in Aspen HYSYS that provided equipment and utility requirements for the system. A table of results including all equipment and their specifications and the HYSYS model schematic are given in Appendices D and E respectively. Aspen economics provided the base modular cost (BMC) of

heat exchanges, pumps, compressors, reactors and separators. Other equipment including the PSA, TSA, H_2S absorber, flare and electrolysers were estimated with consideration of data provided by our industrial partners (Walker Environmental and Integrated Gas Recovery Services - IGRS, Ontario, Canada) and online through information provided by Nel hydrogen [43]. The base modular cost includes the cost of the process unit as well as the installation cost. An additional $2 million was included in the BMC to account for any piping, instrumentation, electrical equipment and building needs. With this consideration, the total BMC for the project was calculated to be $48 million. This value is broken down per unit type in Figure 14. Major contributors to this value can be identified as the electrolysers, PSA unit, and compressors.
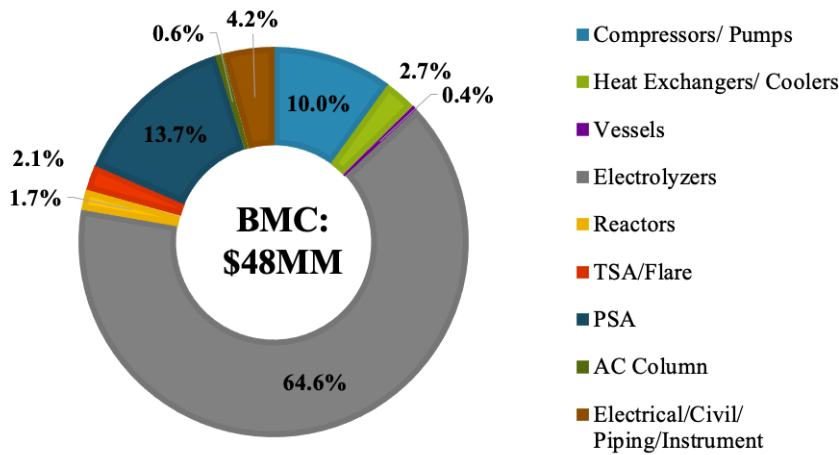
Figure 14. Base modular cost percent breakdown for unit operation type.

$$FCI\ Direct = BMC + Land \tag{28}$$

$$FCI\ Indirect\ = ES + C + CTF + Ct \tag{29}$$

$$TCI = FCI\ Direct + FCI\ Indirect \tag{30}$$

Assuming no land must be purchased, the direct fixed capital investment (FCI) can be calculated though Eq.28 and yields the same value as the BMC equating to $48 million. This

estimate represents the capital cost of all physical assets required for the project. In addition, the project requires consideration of indirect FCI arising from factors such as engineering design, contactor, installation and construction costs and contingency as shown in Eq.29. Since these values cannot be accurately represented in this preliminary design stage, each is estimated as a percentage of the base modular cost. The sum of the indirect and direct FCI as shown by Eq.30 provide the total capital investment (TCI) which comes to $87 million for this facility. A detailed breakdown of the TCI and its contributing components can be seen in Table 4.

Table 4. Breakdown of contributing factors of TCI.

Parameter	Value
Base Modular Cost	55% TCI
Engineering Design	10% TCI
Installation, Construction and Contractor costs	15% TCI
Contingency	20% TCI

Operational expenses for the plant include raw materials, utilities (water and electricity), equipment maintenance and labor. The primary raw input to the system is landfill gas which is assumed to be available free of charge. Utility requirements for the system were determined based on the heat and material balance data provided by HYSYS. Commodity prices are chosen to reflect current market prices and provide an accurate operational cost value. Material costs are provided in Table 5.

Table 5. Material, utility and selling prices of commodities.

Parameter	Value
Selling Price of SNG	$15/GJ - $25/GJ
Water Price	$1/m^3$
Electricity Price	$0.04/kWh – $0.18/kWh
Annual Labour Cost	$100000/Person

Electricity requirements were based on the total power consumption of the system calculated to be 56 MW. Table 6 outlines the contribution of each equipment type to the total power rating of the system. Based on this data, the electrolysers are the main contributor to electricity cost and power consumption by the system. Considering such high-power requirement, a specific electricity price was not selected for the study. Rather, a range of prices was considered to better understand the feasibility limits of the system.

Table 6. Power rating broken down by equipment type.

Equipment	Fraction of Total Power Requirement (%)
Electrolysers	80%
Compressors/Pumps	9%
Glycol Chiller	10%
PSA/TSA	1%

Additional annual costs include labour and maintenance. A staff of 7 professional operators was selected to operate this plant with an annual salary of $80,000 plus 25% burdens (Health and Life Insurance, Pension etc.) for an all in annual cost of $100,000 per operator. Maintenance costs were estimated for the compressors, pump, exchangers and vessels to be approximately 5% of their base modular cost per annum. The remaining equipment required greater detail in maintenance calculations to customize individually for each equipment type. Examples include consideration of column media lifetimes, catalyst for the reactors and electrolyser cell stacks replacements. The total annual operational costs for the abovementioned process were calculated for a typical scenario ($20/GJ SNG selling price and $0.05/kWh electricity price) came to be $27 million, which is broken down by unit type in Figure 15.
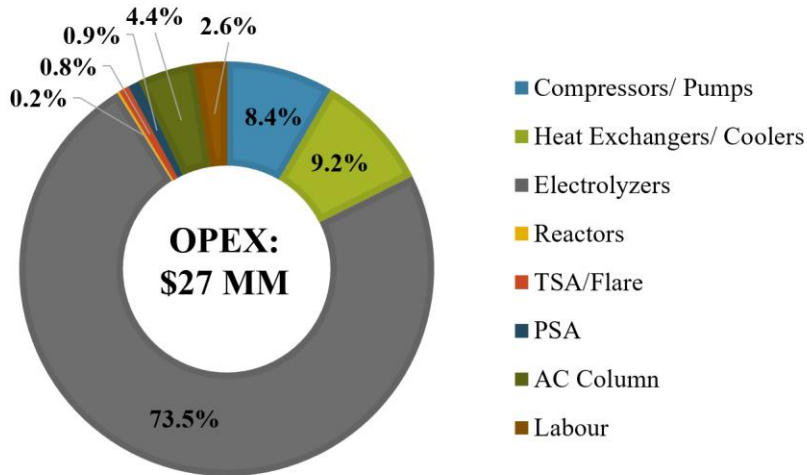
Figure 15. Annual operational cost of synthetic natural production categorized by process equipment type for a typical case ($20/GJ SNG selling price and $0.05/kWh electricity price).

A study briefly discussed in the introduction found the capital investment and operational cost for a 60 SCFM biogas feed system (1.34 MW power rating) to be $5,194,000 (CAD) and $693,377 (CAD) respectively [31]. To compare, these values are scaled linearly to a flowrate of 5000 SCFM and converted to USD. Results show that a 5000 SCFM system to have a $332 million capital investment and an operating cost of $44 million per annum. These values are greater but of similar magnitude to the values found in this study.

Electricity prices in North American cities for residences ranges from $0.06/kWh to $0.24/kWh depending on location [45]. For large scale industries with power demands of 5MW or higher, the rate drops down to $0.04/kWh to $0.18/kWh depending on location [45]. The second range of electricity prices are used for this analysis as the SNG production plant qualifies as a large-scale facility. Production cost as a function of electricity price were calculated using Eq.31 and plotted in Figure 16a. For this study, the tax rate was set to 25% and the plant life (PL) to 20 years. Production costs for SNG range from $13/GJ to $45/GJ. At a selling price of $15/GJ, SNG production is technically feasible at electricity prices at and under $0.05/kWh but the profit margin

is quite small. With a higher selling price of $20/GJ the process is feasible up to electricity prices of $0.07/kWh. Further increase of selling price to $25/GJ increases feasibility up to electricity prices of $0.09/kWh.

A study briefly mentioned in the introduction reported SNG production cost of €1,650,000 per year for a 125 SCFM facility.[8] Assuming the biogas used is of similar composition and undergoes 90% conversion, we can calculate a theoretical production cost to be compared to number obtained in this study. Assuming an exchange rate of 0.89 Euros per USD, the resulting production cost would be approximately $36/GJ. This is within the range found in this study.

$$PC = \frac{TCI + (OC \times PL)}{HHV \times F_{RNG} \times PL} \tag{31}$$
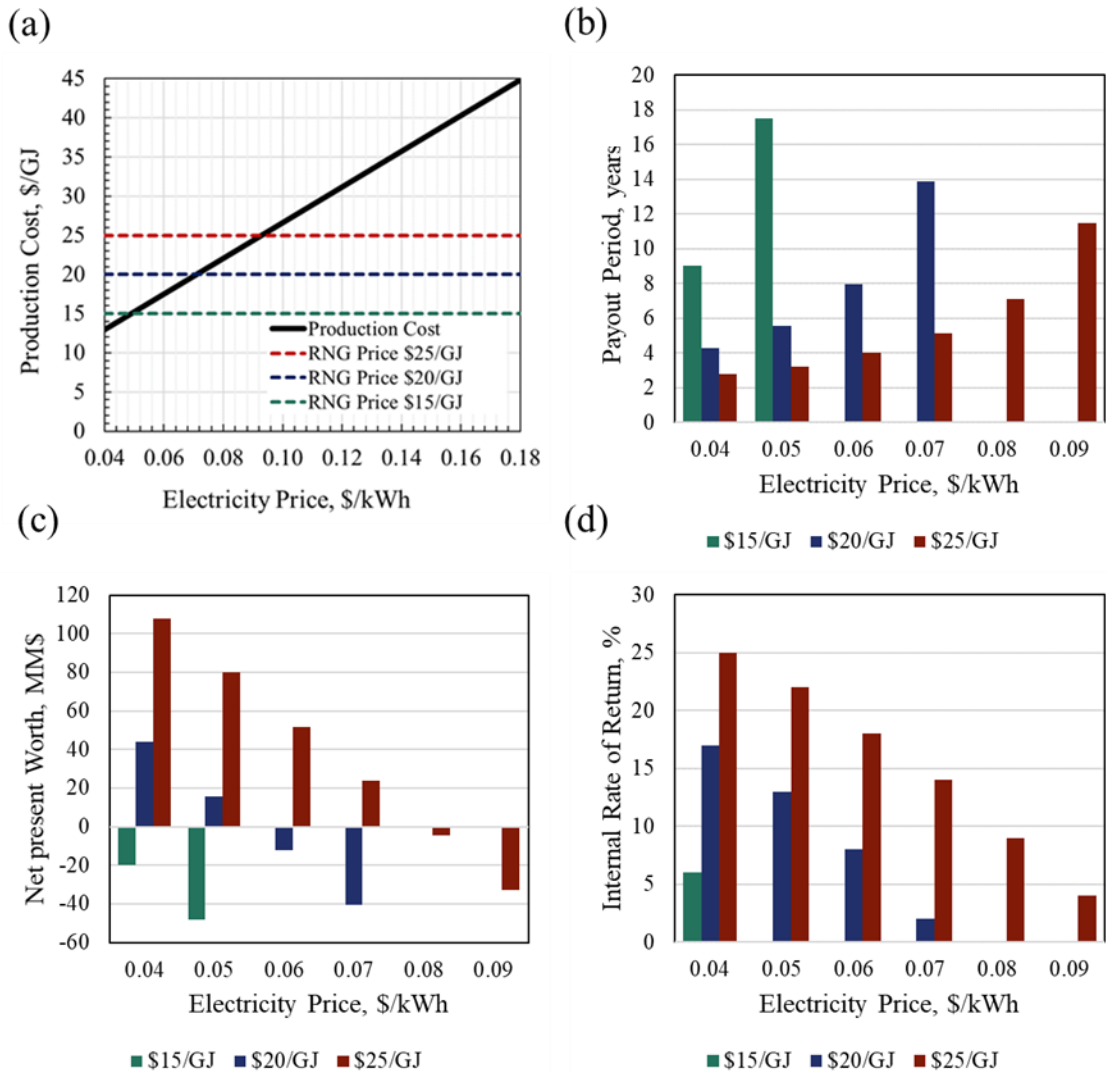
Figure 16. Production cost as a function of electricity price compared to a range of SNG selling prices.

Material balances acquired from HYSYS provide an SNG production rate of 255 GJ/h for the 5000 SCFM system. Assuming a plant uptime of 95%, the revenue was determined by combing the selling price of SNG with the production rate. Further, Eq.32 was utilized to find the profit before tax (PBT). The taxation rate was set to 25% and the depreciation was calculated at 30% per annum with 15% for the first year. Defining these parameters, the profit after tax (PAT) was found using Eq.33. Additionally, Eq.34 and Eq.35 were used to calculate the cash flow (CF) and

cumulative cash flow (CCF) respectively. Figure 17 depicts the CCF as a function of time through the lifetime of the plant for a typical case ($20/GJ SNG selling price and $0.05/kWh electricity price). The economics are promising as a positive CCF is achieved at approximately 7 years post start-up. Setting the discount rate at 10%, the present worth is calculated using Eq.36 and plotted per annum in Figure 17 for a typical case ($20/GJ SNG selling price and $0.05/kWh electricity price). The values are positive every year with the exception of the first year when the capital is paid. This indicated a positive economic outlook without profit loss throughout the plant life. However, these positive values are small in comparison to the capital expenditure predicting the low profit nature of this investment.

$$PBT = Revenue - Total\ Cost \tag{32}$$

$$PAT = PBT - (PBT - Depreciation) \times Tax\ Rate \tag{33}$$

$$CF = PAT - FCI + Salvage\ value \tag{34}$$

$$CCF = \sum_{0}^{PL} CF_n \tag{35}$$

$$PW = \frac{CF}{[1 + i]^n} \tag{36}$$
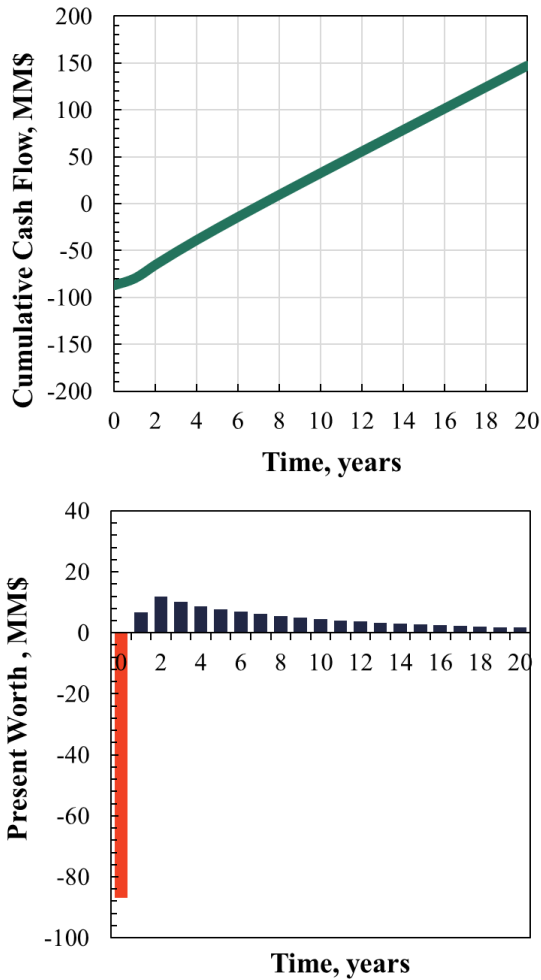
Figure 17. Project cumulative cash flow (upper panel) and present worth (lower panel) presented as a function of plant life per annum for a typical case ($20/GJ SNG selling price and $0.05/kWh electricity price).

Payout periods for the system were calculated using Eq.37 with results presented in Figure 16b. Ideal payout periods should be no more than 25-30% of plant life. This looks to be achievable up to $0.05/kWh at a selling price of $20/GJ and up to $0.07/kWh at a selling price of $25/GJ. Net present worth (NPW) values were determined through Eq.38 with associated results presented in Figure 16c. Positive values of NPW forecast desirable economics with higher values showing

greater promise. Promising NPW values were achieved up to $0.05/kWh at a selling price of $20/GJ and up to $0.07/kWh at a selling price of $25/GJ.A final parameter, the internal rate of return (IRR) was calculated for all profitable scenarios and shown in Figure 16d. Industrial projects typically attract attention when IRR value are above 15% .This is possible up to $0.04/kWh at a selling price of $20/GJ and up to $0.06/kWh at a selling price of $25/GJ.

$$Payout\ Period = \frac{Direct\ FCI}{Profit\ Before\ Tax} \tag{37}$$

$$Net\ Present\ Worth = \sum_{0}^{20} \frac{Profit\ After\ Tax - TCI + Salvage\ Value}{[1+i]^n} \tag{38}$$

This process shows to be feasible only in circumstances where low cost, clean electricity is available. The electrolysis system is undoubtedly the most expensive from both a capital investment and operational cost standpoint. Further technological advancement in the field of water electrolysis are required to significantly reduce associated costs and increase the feasibility of this system. A potential revenue stream may arise from selling the large volumes of high purity oxygen gas produced during electrolysis. Although this additional revenue stream is not considered in this study, its inclusion in future project economics may lead to greater chances of technology adoption. Additionally, the high temperature compressed air stream leaving the cooling compartments of the reactor can be utilized to provide heat to nearby buildings or put though generators to provide some onsite electricity. This can also alleviate some operational expenses and increase feasibility and probability.

4.4.   Renewables

The results presented above consider electricity requirements to be purchased externally from the grid. Rapid changes in the global energy sector provide reason to consider renewable sources as a means for power production. Figure 18 show the altered schematic with the addition of renewable options. A major assumption in this section is that the renewable infrastructure is purchased as a section of the system. As a result, any electricity obtained through renewable means is virtually free for use by the producer. However, the economics does take into consideration capital investment for the renewable electricity generation and any associated maintenance costs. Due to this consideration, power requirements of the system can only be offset in part by renewable sources. The goal of the study is to determine if the system can produce a reasonable profit margin for higher grid electricity prices if a percent of power was produced onsite.
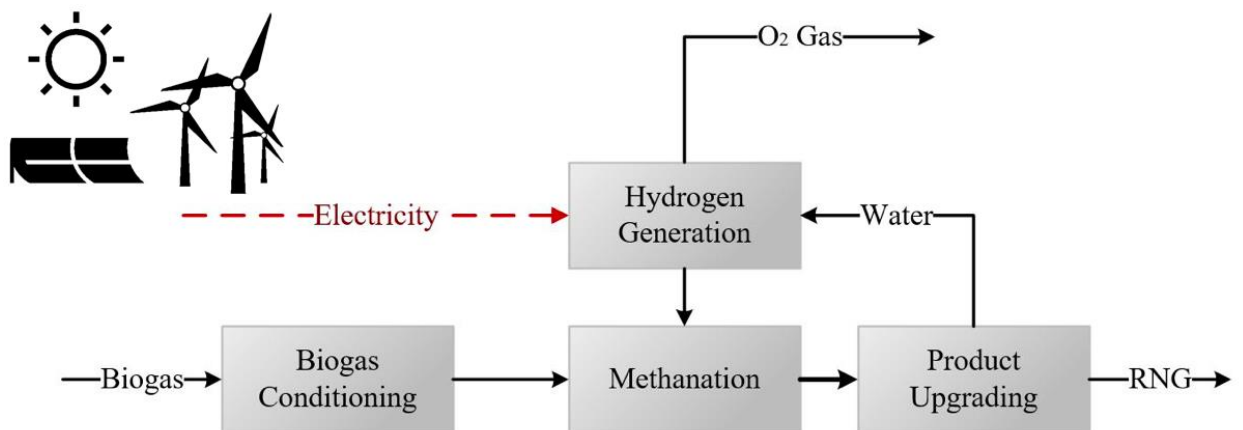
Figure 18. Methanation system overview with renewable energy

4.4.1. *Wind Turbines*

One possible alternative to purchased electricity is wind energy. Wind turbines are highly researched and have been installed extensively worldwide. Global capacities for wind energy have increased from 133.04 TWh in 2006 to 959.53 TWh in 2016 [46]. With growing diversity in the energy sector, wind energy is expected to increase in the coming years. In the following section, a feasibility study will be conducted to assess the economics potential for integrating wind energy with the PtG system. Based on information on current commercial turbines, it is assumed each provides an average 2 MW of power [47]. Each unit is predicted to have an installed capital cost between $3 million and $4 million [47]. For the purpose of this study, it is assumed that the BMC of each unit is $3.5 million. Annual maintenance for each turbine is predicted as 5% of the BMC. As with any energy source, it is crucial that the chosen site have high affinity to wind. Based on this it is assumed that the capacity factor for a given site is 40%. This is within range with typical industry values.

Following these assumptions, the economic model described above was utilized to calculate an overall production cost and project payout period as a function of number of turbines added. Results for this analysis can be seen in Figure 19. When electricity from the grid is cheap at 0.05$/kWh, the introduction of wind energy slightly increases the production cost and payout period. As electricity price increases, wind energy introduces economic benefits with the production costs lowering with a higher slope as electricity prices increase. At 0.07$/kWh, the profit margin is shown to widen with each turbine introduced. The conventionally unprofitable 0.09$/kWh case for a selling price of 20 $/GJ shows to approach the profit line with increased wind investment. Overall, wind energy should be considered as it may result in overall reduction in cost and external energy dependency. It is worth noting that each turbines requires

51

approximately 500 m of distance from any other turbines or structure. Therefore, a large area must

be allocated for wind energy if this option were to be considered.
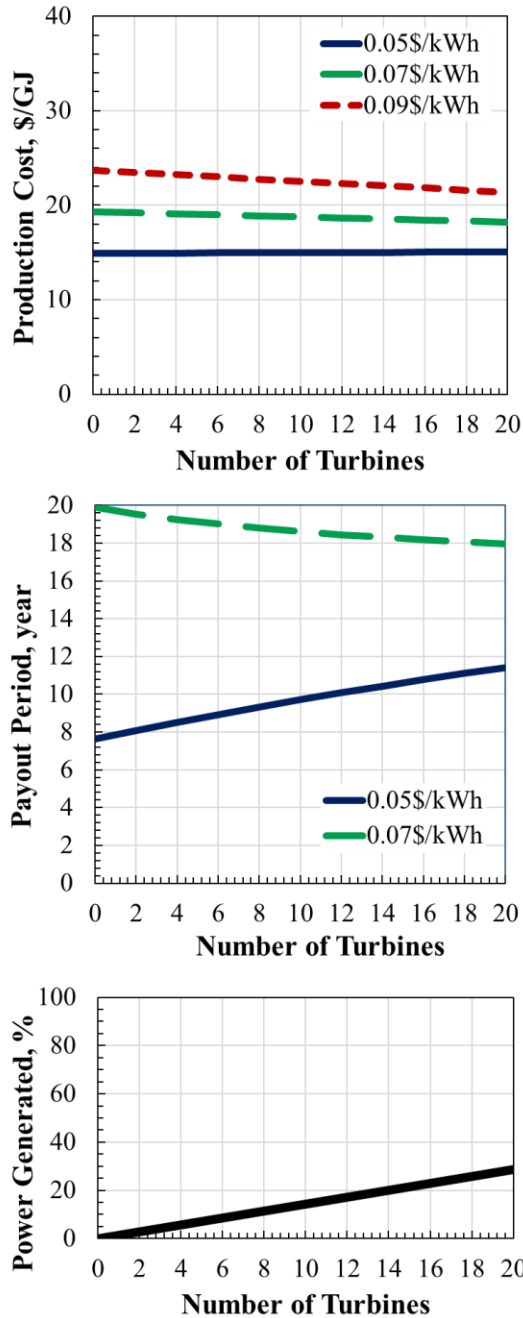
Figure 19. SNG production cost (upper panel) payout period (middle panel) and % power

generated (lower panel) for installing wind turbines at the project site.

4.4.2.   Solar Panels

An alternative for renewable source to provide electricity to this PtG system is solar energy. This section assesses the technical and economic feasibility of solar panels for onsite electricity production. Due to intermittency and availability, it is important to consider the geographic location of the site prior to consideration of solar energy solutions. Based on typical industry information on current panels, the rating and BMC are chosen at 320W and $960 respectively [48]. A single panel in this study is considered to have an area of 1.5 m^2 [48]. As with the turbines, the annual maintenance cost is assumed to be 5% of the BMC. Since the sunlight is not available at full capacity all year, a factor was taken to account for this intermittency. Based on information provided for average equivalent full sunlight hours in Canada [49], it was assumed that an average 10% of the total rating would be available year long.

Following these assumptions, the economic model described above was utilized to calculate an overall production cost and project payout period as a function of number of panels added. Results for this analysis can be seen in Figure 20. All scenarios studied showed an increased SNG production cost with inclusion of solar energy. This indicates that power generated per panel does not decrease the overall operating cost enough to justify the capital expenditure. In line with this trend, the payout period for all cases is increased due to solar panel introduction. With the high capital expenditures and low energy gains, solar energy may not be the best solution for onsite electricity production.
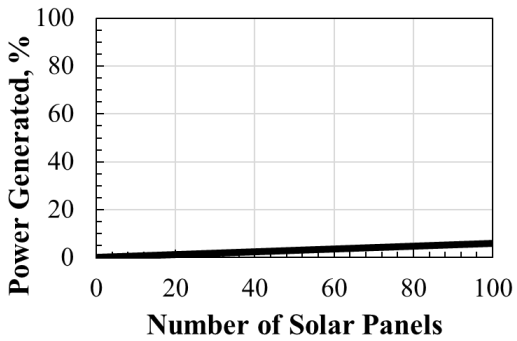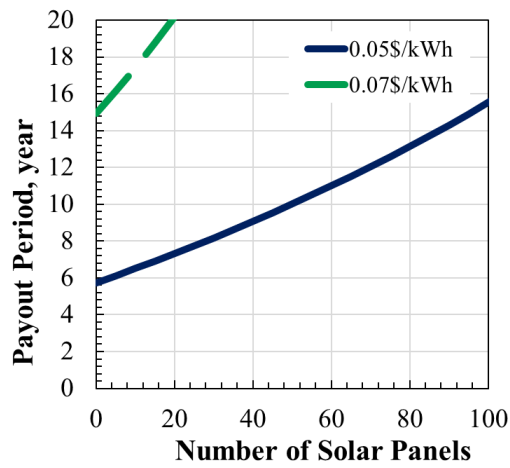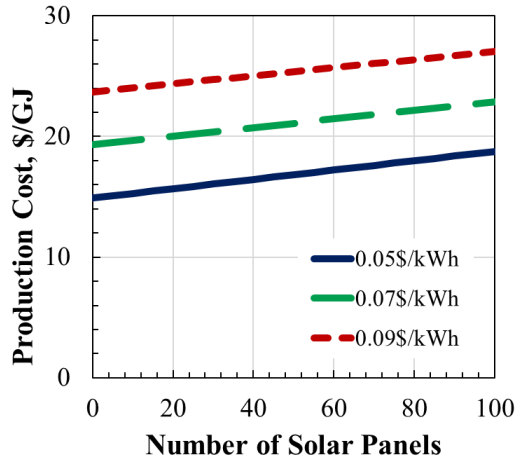
Figure 20. SNG production cost (Upper Panel), power generated (middle panel) and area required (lower panel) for installing solar panels at the project site

5. Concluding Remarks

5.1.   Conclusion

This study successfully synthesized a process for the production of pipeline grade SNG from a raw landfill gas feed. Feed biogas was conditioned through use of a desulphurization skids, dehydration unit, and temperature swing adsorption for VOC and siloxane removal. The reaction system consisted of parallel Sabatier reactors fed by conditioned biogas and hydrogen produced via water electrolysis. Upgrading technologies utilized included a pressure swing adsorption unit and a dehydration skid for removal of nitrogen gas and water respectively. A mathematical model of the reactor system was developed and optimized in MATLAB. This model was then retrofit to a process model in HYSYS to define process stream and determine flow requirements.

Resulting techno-economic assessment predicted the base modular cost and total capital investment required for the project to be $48 million and $87 million respectively. SNG production costs were calculated to vary between $13/GJ to $45/GJ, depending on commodity prices with great reliance on the price of electricity. This is comparable to the production cost of synthetic natural gas via CO_2 and CH_4 separation which is reported as 10-15$/GJ (Walker Environmental and Integrated Gas Recovery Services - IGRS, Ontario, Canada). Production values reported are higher than fossil natural gas prices but comparable to liquefied natural gas production costs. The technology is considered attractive in locations where fossil natural gas in not readily available. Sensitivities on electricity prices between $0.04/kWh to $0.18/kWh were conducted to better understand the effect of this commodity on production cost. Further economic analysis on all profitable cases allowed for calculation of more sophisticated factors such as net present worth, payout period and internal rate of return for the project.

This analysis shed light on the economically attractive scenarios for the SNG production project. The system was predicted to be economically viable only under circumstances where low cost electricity is available. The electrolysis system was found to be responsible for 65% of the base modular cost and approximately 74% of operational expenditures with the contributions of the methanation system being negligible. Best economic scenarios resulted from electricity prices up to $0.04/kWh at a selling price of $20/GJ and up to $0.06/kWh at a selling price of $25/GJ. These scenarios presented the best payout periods, positive NPW values and IRRs above 15%.

5.2.   *Future Work*

Further work is required optimize both the reactor configuration and system design to enhance the feasibility of the project. Development of 2D and 3D mathematical models of the proposed reactor designs to evaluate the presence and severity of radial gradients within each reactor should be completed. Additionally, experimental results for a pilot scale reactor should be gathered to better understand the effects of scale up on the reactor and determine the validity of the numerical models (MATLAB and HYSYS). Equipment optimization is key to increased feasibility. Recycle opportunities for both heat and material streams must be further integrated into the model to reduce overall power consumption and cost. Further investigation should consider cheap intermittent electricity use for production and storage hydrogen in order to improve economics.

Investigation of economics using various sources of carbon should be undertaken to clarify the range of feasibility for this technology. Additionally, the variability of feed compositions should be investigated to have a more realistic understanding of an up and running plant. Integration of profit from oxygen sales can highly improve the economics of the system. Further analysis must

investigate uses for this high purity oxygen product. These future investigations will allow for further clarification of technical and economic feasibility of the described methanation system.

Pilot demonstration of this unit is required in the future to assess real operating requirements for equipment as well as reactor performance at industrial scales. The feasibility of a pilot study depends heavy on environmental incentives provided to industry by government organizations with goals of reducing GHG emissions and increase renewable sources. Additionally, the success of this industry is linked to the price and availability of fossil natural gas. SNG prospects show greater promise in geographical areas with limited access to inexpensive and abundant fossil natural gas.

6. References

[1] Association CB. Renewable Natural Gas Developments in Ontario An Evolving Outlook. 2017.

[2] Aresta M, Dibenedetto A. Utilisation of CO2 as a chemical feedstock: opportunities and challenges. Dalton Trans. 2007:2975-92.

[3] Wang W, Wang SP, Ma XB, Gong JL. Recent advances in catalytic hydrogenation of carbon dioxide. Chem Soc Rev. 2011;40:3703-27.

[4] Simakov DSA. Renewable synthetic fuels and chemicals from carbon dioxide. New York, NY: Springer International Publishing 2017.

[5] Gotz M, Lefebvre J, Mors F, Koch AM, Graf F, Bajohr S, et al. Renewable Power-to-Gas: A technological and economic review. Renewable Energy. 2016;85:1371-90.

[6] Re F, Toro C, Sciubba E. Sabatier Based Cycle for Co2 Methanation: Exergy and Thermo-Economic Analysis. Proceedings of the Asme International Mechanical Engineering Congress and Exposition, 2017 Vol 6. 2018.

[7] Ronsch S, Schneider J, Matthischke S, Schluter M, Gotz M, Lefebvre J, et al. Review on methanation - From fundamentals to current projects. Fuel. 2016;166:276-96.

[8] Collet P, Flottes E, Favre A, Raynal L, Pierre H, Capela S, et al. Techno-economic and Life Cycle Assessment of methane production via biogas upgrading and power to gas technology. Appl Energy. 2017;192:282-95.

[9] Guilera J, Morante JR, Andreu T. Economic viability of SNG production from power and CO2. Energy Convers Manage. 2018;162:218-24.

[10] Baumann C, Schuster R, Moser A. Economic potential of power-to-gas energy storages. 2013 10th International Conference on the European Energy Market (EEM)2013. p. 1-6.

[11] de Boer HS, Grond L, Moll H, Benders R. The application of power-to-gas, pumped hydro storage and compressed air energy storage in an electricity system at different wind power penetration levels. Energy. 2014;72:360-70.

[12] Hashimoto K, Yamasaki M, Fujimura K, Matsui T, Izumiya K, Komori M, et al. Global CO2 recycling - novel materials and prospect for prevention of global warming and abundant energy supply. Materials Science and Engineering a-Structural Materials Properties Microstructure and Processing. 1999;267:200-6.

[13] Jentsch M, Trost T, Sterner M. Optimal Use of Power-to-Gas Energy Storage Systems in an 85% Renewable Energy Scenario. 8th International Renewable Energy Storage Conference and Exhibition (Ires 2013). 2014;46:254-61.

[14] Plessmann G, Erdmann M, Hlusiak M, Breyer C. Global energy storage demand for a 100% renewable electricity supply. 8th International Renewable Energy Storage Conference and Exhibition (Ires 2013). 2014;46:22-31.

[15] Mills GA, Steffgen FW. Catalytic Methanation. Catal Rev. 1974;8:159-210.

[16] Bartholomew CH. Catalyst Deactivation and Regeneration. Kirk-Othmer Encyclopedia of Chemical Technology2003.

[17] Agnelli M, Kolb M, Mirodatos C. Co Hydrogenation on a Nickel-Catalyst .1. Kinetics and Modeling of a Low-Temperature Sintering Process. Journal of Catalysis. 1994;148:9-21.

[18] Gierlich HH, Fremery M, Skov A, Rostrup-Nielsen JR. Deactivation Phenomena of a Ni-based Catalyst for High Temperature Methanation. In: Delmon B, Froment GF, editors. Studies in Surface Science and Catalysis: Elsevier; 1980. p. 459-69.

[19] Struis RPWJ, Schildhauer TJ, Czekaj I, Janousch M, Biollaz SMA, Ludwig C. Sulphur poisoning of Ni catalysts in the SNG production from biomass: A TPO/XPS/XAS study. Applied Catalysis a-General. 2009;362:121-8.

[20] Frusteri F, Spadaro L, Arena F, Chuvilin A. TEM evidence for factors affecting the genesis of carbon species on bare and K-promoted Ni/MgO catalysts during the dry reforming of methane. Carbon. 2002;40:1063-70.

[21] Currie R, Mottaghi-Tabar S, Zhuang Y, Simakov DSA. Design of an Air-Cooled Sabatier Reactor for Thermocatalytic Hydrogenation of CO2: Experimental Proof-of-Concept and Model-Based Feasibility Analysis. Ind Eng Chem Res. 2019.

[22] Sun D, Simakov DSA. Thermal management of a Sabatier reactor for CO2 conversion into CH4: Simulation-based analysis. J CO2 Util. 2017;21:368-82.

[23] Brooks KP, Hu JL, Zhu HY, Kee RJ. Methanation of carbon dioxide by hydrogen reduction using the Sabatier process in microchannel reactors. Chem Eng Sci. 2007;62:1161-70.

[24] Junaedi C, Hawley K, Vilekar SA, Roychoudhury S. Evaluation of CO2 Adsorber, Sabatier Reactor, and Solid Oxide Stack for Consumable, Propellant, and Power Production Potential in ISRU Architecture. 46th International Conference on Environmental Systems. Vienna, Austria2016.

[25] Junaedi C, Hawley K, Walsh D, Roychoudhury S, Abney M, Perry J. CO2 Reduction Assembly Prototype using Microlith-based Sabatier Reactor for Ground Demonstration. 44th International Conference on Environmental Systems Tucson, Arizona2014.

[26] Sudiro M, Bertucco A, Groppi G, Tronconi E. Simulation of a structured catalytic reactor for exothermic methanation reactions producing synthetic natural gas. 20th European Symposium on Computer Aided Process Engineering. 2010;28:691-6.

[27] Kopyscinski J, Schildhauer TJ, Biollaz SMA. Fluidized-Bed Methanation: Interaction between Kinetics and Mass Transfer. IndEng Chem Res. 2011;50:2781-90.

[28] Seemann MC, Schildhauer TJ, Biollaz SMA. Fluidized Bed Methanation of Wood-Derived Producer Gas for the Production of Synthetic Natural Gas (vol 49, pg 7034, 2010). Ind Eng Chem Res. 2010;49:11119-.

[29] Götz M, Ortloff F, Reimert R, Basha O, Morsi BI, Kolb T. Evaluation of Organic and Ionic Liquids for Three-Phase Methanation and Biogas Purification Processes. Energy Fuels. 2013;27:4705-16.

[30] Lefebvre J, Gotz M, Bajohr S, Reimert R, Kolb T. Improvement of three-phase methanation reactor performance for steady-state and transient operation. Fuel Process Technol. 2015;132:83-90.

[31] Walker SB, Sun D, Kidon D, Siddiqui A, Kuner A, Fowler M, et al. Upgrading biogas produced at dairy farms into renewable natural gas by methanation. Int J Energy Res. 2018;42:1714-28.

[32] Vo TTQ, Wall DM, Ring D, Rajendran K, Murphy JD. Techno-economic analysis of biogas upgrading via amine scrubber, carbon capture and ex-situ methanation. Appl Energy. 2018;212:1191-202.

[33] Sun D, Khan FM, Simakov DSA. Heat removal and catalyst deactivation in a Sabatier reactor for chemical fixation of CO2: Simulation-based analysis. Chem Eng J. 2017;329:165-77.

[34] Schlereth D, Hinrichsen O. A fixed-bed reactor modeling study on the methanation of CO2. Chem Eng Res Des. 2014;92:702-12.

[35] Simakov DSA, Sheintuch M. Design of a thermally balanced membrane reformer for hydrogen production. Aiche J. 2008;54:2735-50.

[36] Simakov DSA, Sheintuch M. Model-Based Optimization of Hydrogen Generation by Methane Steam Reforming in Autothermal Packed-Bed Membrane Reformer. Aiche J. 2011;57:525-41.

[37] Janz GJ. Molten Salts Handbook. New York: Elsevier; 1967.

[38] Mills AF. Heat Transfer: Irwin; 1992.

[39] Morrell R. Handbook of properties of technical & engineering ceramics. London: Her Majesty's Stationery Office; 1985.

[40] Touloukian YS, Kirby RK, Taylor ER, Lee TYR. Thermophysical properties of matter: Purdue University; 1977.

[41] Chen XY, Vinh-Thang H, Ramirez AA, Rodrigue D, Kaliaguine S. Membrane gas separation technologies for biogas upgrading. Rsc Advances. 2015;5:24399-448.

[42] TransCanada. Gas Quality Specifications TransCanada and other pipelines. 2018. p. http://www.tccustomerexpress.com/docs/Gas_Quality_Specifications_Fact_Sheet.pdf.

[43] NelHydrogen. Nel Hydrogen Electrolyser The world's most efficient and reliable electrolyser. In: NelHydrogen, editor.: NelHydrogen; 2017.

[44] Aspen Technology I. Aspen HYSYS Manual V8.8: Aspen Technology, Inc.; 2015.

[45] Quebec H. Comparison of Electricity Prices in Major North American Cities. 2018.

[46] Ritchie H, Roser M. Global renewable energy consumption over the long-run.

[47] Windustry. How much do wind turbines cost. 2012.

[48] Zientara B. How much electricity does a solar panel produce.

[49] energyhub. Cost of Solar Power In Canada 2019. 2019.

[50] Xu JG, Froment GF. Methane Steam Reforming, Methanation and Water-Gas Shift .1. Intrinsic Kinetics. Aiche J. 1989;35:88-96.

[51] Wu SH, McAuley KB, Harris TJ. Selection of Simplified Models: Ii. Development of a Model Selection Criterion Based on Mean Squared Error. Can J Chem Eng. 2011;89:325-36.

[52] Elnashaie SSEH, Adris AM, Alubaid AS, Soliman MA. On the Non-Monotonic Behavior of Methane Steam Reforming Kinetics. Chem Eng Sci. 1990;45:491-501.

[53] Simakov DSA, Luo HY, Román-Leshkov Y. Ultra-low loading Ru/γ-Al$_2$O$_3$: A highly active and stable catalyst for low temperature solar thermal reforming of methane. Appl Catal B: Environ. 2015;168-169:540-9.

[54] Mears DE. Tests for Transport Limitations in Experimental Catalytic Reactors. Ind Eng Chem Proc Dd. 1971;10:541-&.

[55] Frössling N. Uber die Verdunstung fallender Tropfen. Gerlands Beitr Geophys. 1938;52:170-216.

[56] Ranz WE, Marshall WR. Evaporation from Droplets: part I and II. Chem Eng Prog. 1952;48:141-73.

[57] Froment GF, Bischoff KB. Chemical Reactor Analysis and Design: Wiley; 1979.

[58] Berger RJ, Perez-Ramirez J, Kapteijn F, Moulijn JA. Catalyst performance testing - Radial and axial dispersion related to dilution in fixed-bed laboratory reactors. Appl Catal A-Gen. 2002;227:321-33.

[59] Derkx OR, Dixon AG. Effect of the wall Nusselt number on the simulation of catalytic fixed bed reactors. Catal Today. 1997;35:435-42.

[60] Dixon AG, Cresswell DL. Theoretical Prediction of Effective Heat-Transfer Parameters in Packed-Beds. Aiche J. 1979;25:663-76.

[61] Gnielinski V. New Equations for Heat and Mass-Transfer in Turbulent Pipe and Channel Flow. Int Chem Eng. 1976;16:359-68.

[62] Holman JP. Heat transfer. 9 ed. New York: McGraw-Hill; 2002.

[63] Sergeev OA, Shashkov AG, Umanskii AS. Thermophysical properties of quartz glass. J Eng Phys Thermophys. 1982;43:1375-83.

[64] Churchill SW, Chu HHS. Correlating Equations for Laminar and Turbulent Free Convection from a Horizontal Cylinder. Int J Heat Mass Tran. 1975;18:1049-53.

Appendices

A. *Reaction rate expressions*

A Ni/Al$_2$O$_3$ catalyst was selected for the reaction (packed bed) compartment. Reaction rate expressions from the literature were implemented, Eq. A1 to Eq. A3 [50]. These kinetic expressions, although originally developed for methane steam reforming, account for the reversibility of all reactions involved. Therefore, it is expected that Eq. A1 to Eq. A3 can describe the Sabatier-CO methanation-reverse water gas shift reaction system described by Eq. A1 to Eq. A3. This assumption was experimentally validated using a commercial Ni catalyst (12 wt% Ni/Al$_2$O$_3$, BASF, supplied by Research Catalysts, Inc. USA); kinetic parameters were estimated through the non-linear least squares regression.

$$R_1 = \frac{k_1}{p_{H_2}^{2.5}} \left(p_{CH_4} p_{H_2O} - \frac{p_{H_2}^3 p_{CO}}{K_{1,eq}} \right) \frac{1}{\text{den}^2} \tag{A1}$$

$$R_2 = \frac{k_2}{p_{H_2}} \left(p_{CO} p_{H_2O} - \frac{p_{H_2} p_{CO_2}}{K_{2,eq}} \right) \frac{1}{\text{den}^2} \tag{A2}$$

$$R_3 = \frac{k_3}{p_{H_2}^{3.5}} \left(p_{CH_4} p_{H_2O}^2 - \frac{p_{H_2} p_{CO_2}}{K_{3,eq}} \right) \frac{1}{\text{den}^2} \tag{A3}$$

$$\text{den} = 1 + K_{CO} p_{CO} + K_{H_2} p_{H_2} + K_{CH_4} p_{CH_4} + \frac{K_{H_2O} p_{H_2O}}{p_{H_2}}$$

$$k_j = A_j \exp\left(\frac{-E_j}{R_g T} \right) \qquad K_i = B_i \exp\left(\frac{-\Delta H_i}{R_g T} \right) \qquad K_{j,eq} = B_j \exp\left(\frac{-\Delta H_j}{R_g T} \right)$$

B. Reaction rate expressions

To estimate the parameters in Eq. A1 to Eq. A3 (A_j, E_j, B_i and $\varDelta H_i$, total 14 parameters), a set of lab experiments were carried out to monitor the change in species concentrations as a function of temperature and space velocity. CO_2 and H_2 were fed by mass flow controllers to a flow reactor containing 0.5g of the catalyst (12 wt% Ni/Al_2O_3, BASF, supplied by Research Catalysts, Inc. USA), with the outlet concentrations monitored using an infrared analyzer (IR-208, Infrared Industries). Parameter estimation was done by minimizing the sum of the squared residuals of the CO_2, CO and CH_4 concentrations by means of the Trust-Region Reflective Algorithm.[51] Simulated mole fractions were obtained by integrating a set of ordinary differential equations (MATLAB ode15s) described by Eq. A4:

$$\varepsilon \frac{dC_i}{dt} = -\varepsilon v_g \frac{\left(C_i - C_{i,f}\right)}{L} + \rho_c (1-\varepsilon) \sum_j \alpha_i R_{ij} \tag{A4}$$
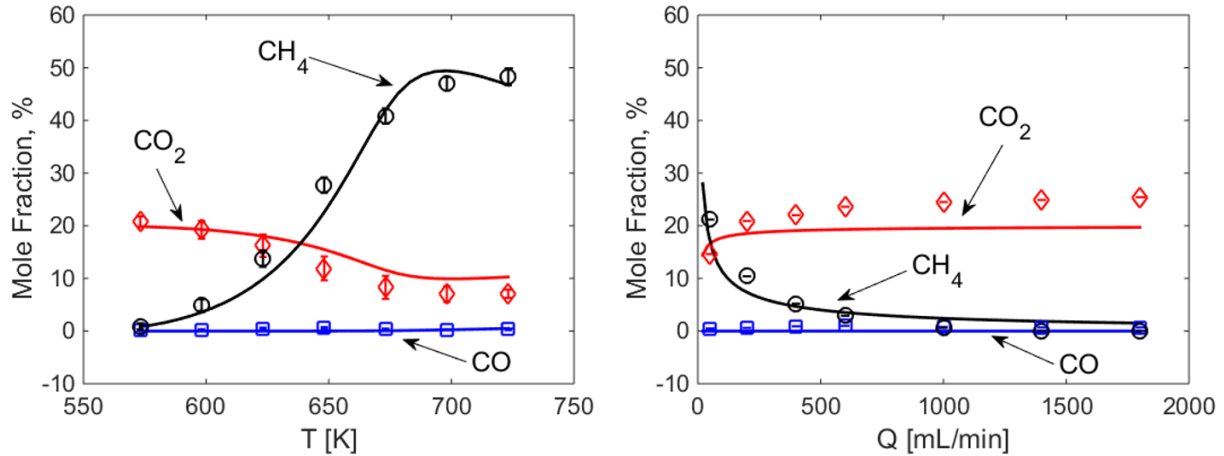
Figure 21. Parameter estimation results, showing the experimentally measured mole fractions (solid lines) and the model prediction (symbols) obtained by integrating Eq. A4 using the estimated parameters.

Eq.A4 represents the time evolution of all species participating in the reaction system in a kinetic flow reactor. Initial guesses for the reaction and adsorption constants were adopted from Xu and Froment [50, 52]. The parameter estimation results are shown in Figure 20, with the estimated parameters listed in Table 7. As it can be seen from Figure 20, the adopted rate expressions with the estimated parameters listed in Table 7 satisfactorily predicts the experimentally measured mole fractions of CO_2, CO and CH_4. Note that the parameter estimation predicts that CH_4 formation pathway is reverse water gas shift with subsequent methanation rather than direct methanation of CO_2.

Table 7. Estimated kinetic parameters.

A_1	A_2	A_3	B_{CO}	B_{H_2}	B_{CH_4}	B_{H_2O}
8.90e8	3.42e6	9.22e-5	1.50e-9	1.86e-12	5.48e-7	6.43e3

E_1	E_2	E_3	ΔH_{CO}	ΔH_{H_2}	ΔH_{CH_4}	ΔH_{H_2O}
122.4	93.1	104.8	-97.3	-103.4	-57.7	104.4

Units of activation energies and adsorption enthalpies are kJ/mol. A_1 and A_2 have units of (mol $kPa^{0.5}$)/(kg s). Units of A_2 are mol/(kPa kg s).

C. Transport Parameters

Intra-particle and interphase mass and heat transfer limitations were assessed using the following criteria [53, 54]:

$$\phi_j^2 = \frac{\hat{k}_j d_p^2}{4D_m} << 1 \tag{A5}$$

$$\frac{\varepsilon\rho_g \left|\Delta H_{RWGS}\right| \hat{k}_j d_p^2}{4k_s T} << \frac{0.75 TR_g}{E_a} \tag{A6}$$

$$\frac{\hat{k}_j d_p}{2y_{CO_2,f} k_c} << 0.15 \tag{A7}$$

$$\frac{\varepsilon\rho_g \left|\Delta H_{RWGS}\right| \hat{k}_j d_p}{2h_{gs} T} << \frac{0.75 TR_g}{E_a} \tag{A8}$$

$$\hat{k}_1 = \frac{k_1 \rho_s (1-\varepsilon)}{\sqrt{P_{tf}}\, \rho_g \varepsilon} \qquad \hat{k}_2 = \frac{k_2 \rho_s (1-\varepsilon) P_{tf}}{\rho_g \varepsilon} \qquad \hat{k}_3 = \frac{k_3 \rho_s (1-\varepsilon)}{\sqrt{P_{tf}}\, \rho_g \varepsilon}$$

In the equations above, k_s is the thermal conductivity of the pellet which was assumed to be the same as for alumina and calculated using an empirical correlation.[39] The gas mass transfer coefficient (k_c) was calculated from the Sherwood number, estimated by the Frossling correlation,[55] Eq.A9. The effective gas heat transfer coefficient (h_{gs}) was calculated from the Nusselt number, estimated by the analogous correlation for heat transfer,[56] Eq.A10.

$$Sh = \frac{k_c d_p}{D_m} = 2 + 0.6\,\mathrm{Re}^{0.5}\,\mathrm{Sc}^{\frac{1}{3}} \qquad \mathrm{Re}_p = \frac{v_g \rho_g d_p}{\mu_g} \qquad Sc = \frac{\upsilon}{D_m} \tag{A9}$$

$$Nu_p = \frac{h_{gs} d_p}{k_t} = 2 + 0.6\,\mathrm{Re}^{0.5}\,\mathrm{Pr}^{\frac{1}{3}} \qquad \mathrm{Pr} = \frac{\upsilon}{\alpha_t} \tag{A10}$$

Under relevant conditions (600-800 K, 5-10 bar, gas velocity of 0.04-0.2 m/s), and using previously estimated kinetic parameters, it was shown that inter-particle and interphase transport limitations are negligible for methanation reactions. On the other hand, for the reverse water gas shift reaction the intra-particle mass transfer resistance was found to be significant. To account for

that transport limitation the internal effectiveness factor was calculated (for all reactions), using the standard expression for a spherical pellet [57]:

$$\eta_j = \frac{3}{\phi_j}\left(\frac{1}{\tanh\phi_j} - \frac{1}{\phi_j}\right) \qquad\qquad \phi_j = \sqrt{\frac{\hat{k}_j d_p^2}{4 D_m}} \qquad\qquad (A11)$$

Axial mass and heat dispersion in a packed bed were accounted for through the following correlations:

$$D_{ae} = \varepsilon\left(\frac{D_m}{\tau_b} + 0.5 d_p v_g\right) \qquad \tau_b = \frac{1}{\varepsilon^{0.5}} \qquad\qquad (A12)$$

$$k_{ae} = \lambda_g\left(8 + 0.05\,\mathrm{Re}_p^{1.09}\right) \qquad\qquad (A13)$$

The effective axial mass dispersion coefficient, Eq.A12, was calculated using a typical correlation adopted from the literature.[58] The expression for the effective axial heat dispersion coefficient, Eq.A13, was derived from the heat conductivity correlations developed for catalytic fixed beds,[59, 60] by plotting k_{ae} vs. Re_p in the relevant range and least squares fitting.[22]

Wall heat transfer coefficients for heat exchange between the packed bed and cooling tube, Eq.A14, and heat loss to the environment, Eq.A15, were calculated by resistances in series. These parameters account for the contribution of the packed bed (h_{wr}), cooling tube or reactor wall (λ_w), molten salt (h_{wc}), insulation layer (λ_{iw}), and natural convection from the external reactor surface (h_{nc}).

$$U_{w,HE} = \left(\frac{1}{h_{wr}} + \frac{d_w}{\lambda_w} + \frac{1}{h_{wc}}\right)^{-1} \qquad\qquad (A14)$$

$$U_{w,HL} = \left(\frac{1}{h_{wr}} + \frac{d_w}{\lambda_w} + \frac{d_{iw}}{\lambda_{iw}} + \frac{1}{h_{nc}} \right)^{-1} \tag{A15}$$

The effective wall heat transfer coefficient for the reaction compartment (h_{wr}) was estimated using the following correlation:

$$Nu_p = \frac{h_{wr}d_p}{\lambda_g} = 24 + 0.34\,\mathrm{Re}_p^{0.77} \tag{A16}$$

This expression was obtained in the similar way as Eq. A13, using a complete set of the original correlations [59, 60] and least squares fitting [22]. The effective wall heat transfer coefficient for the coolant tube (h_{wc}) was estimated using the following correlations from the literature [38, 61, 62]:

$$\mathrm{Re}_c < 2030 \qquad\qquad Nu_c = 3.66 + \frac{0.065\,\mathrm{Re}_c\,\mathrm{Pr}_c\,(D_c/L)}{1 + 0.04[\mathrm{Re}_c\,\mathrm{Pr}_c\,(D_c/L)]^{2/3}} \tag{A17}$$

$$2030 < \mathrm{Re}_c < 4000 \qquad Nu_c = 0.012(\mathrm{Re}_c^{0.87} - 280)\,\mathrm{Pr}_c^{0.4}\left[1 + (D_c/L)^{2/3}\right] \tag{A18}$$

$$\mathrm{Re}_c > 4000 \qquad\qquad Nu_c = 0.027\,\mathrm{Re}_c^{0.8}\,\mathrm{Pr}_c^{1/3} \tag{A19}$$

$$Nu_c = \frac{h_{wc}D_c}{\lambda_c} \qquad\qquad \mathrm{Re}_c = \frac{v_c\rho_c D_c}{\mu_c} \qquad\qquad \mathrm{Pr}_c = \frac{C_{pc}\mu_c}{\lambda_c}$$

The values for the insulation layer (quartz wool) conductivity (λ_{iw}) and natural convection (h_{nc}) were adopted from the literature [63, 64]. These contributions were dominant in Eq.A15 and the wall heat loss coefficient was nearly constant in all simulations: $U_{w,HL} \approx 0.01$ W/(m^2 K).

D. Detailed Process Parameters

Table 8. Summary of process streams, power ratings and associated costs ($20/GJ SNG selling price and $0.05/kWh electricity price).

Unit	Total Size (m3)	Process Stream (Sm³/h)	No. of Units	Base Modular Cost (1000 USD)	Operational Cost (1000 USD/yr)	Total Power/ Duty (kW)	Reference
Compressors & Pumps							
Biogas Compressor	19	8,817	1	$1,170	$293	563	HYSYS
Air Compressor	164	35470	2	$3,551	$1,983	4340	HYSYS
Glycol Pump	0.02	65	1	$49	$3	0.5	HYSYS
Heat Exchangers							
H2 Pre-Heater	0.52	10,510	1	$135	$7	521	HYSYS
LFG Pre-Heater	0.5	8,817	1	$136	$7	501	HYSYS
SNG Cooler 1	0.95	14,520	1	$250	$12	800	HYSYS
SNG Cooler 2	2.86	14,520	2	$307	$15	3317	HYSYS
Feed Re-heater	0.26	8,816	1	$109	$5	176	HYSYS
Feed Chiller	1.61	8,966	1	$196	$10	190	HYSYS
Glycol Refrigerator	9.4	65	1	$140	$2,449	5870	HYSYS
Methanation Reactor	5.3	19,330/14,520[1]	50	$791	$49	-	HYSYS
Electrolysis System	47250	9.1/10,510[1]	21	$31,787	$20,019	44620	NEL Hydrogen
Separators							
Feed Water KO Drum	2.9	8,966/8,817[1]	1	$94	$5	-	HYSYS
Product Water KO Drum	2.9	14,520/9,677[1]	1	$106	$5	-	HYSYS
TSA	100	8,817	1	$1000	$120	300	IGRS
PSA	100	9,677/6,597[1]	1	$6,500	$250	400	IGRS
AC Column	86	8,817	2	$300	$1,200	-	IGRS
Purge Flare	-	variable	1	$150	$5	-	IGRS
Electrical/ Instrumentation/ Civil/Piping	-	-	-	$2,000	-	-	IGRS
Total			**90**	**$47,769**	**$26,522**	**56,093**	

[1] Flow rate varies changes within the process unit. First number represents the inlet while the second number represents the outlet.
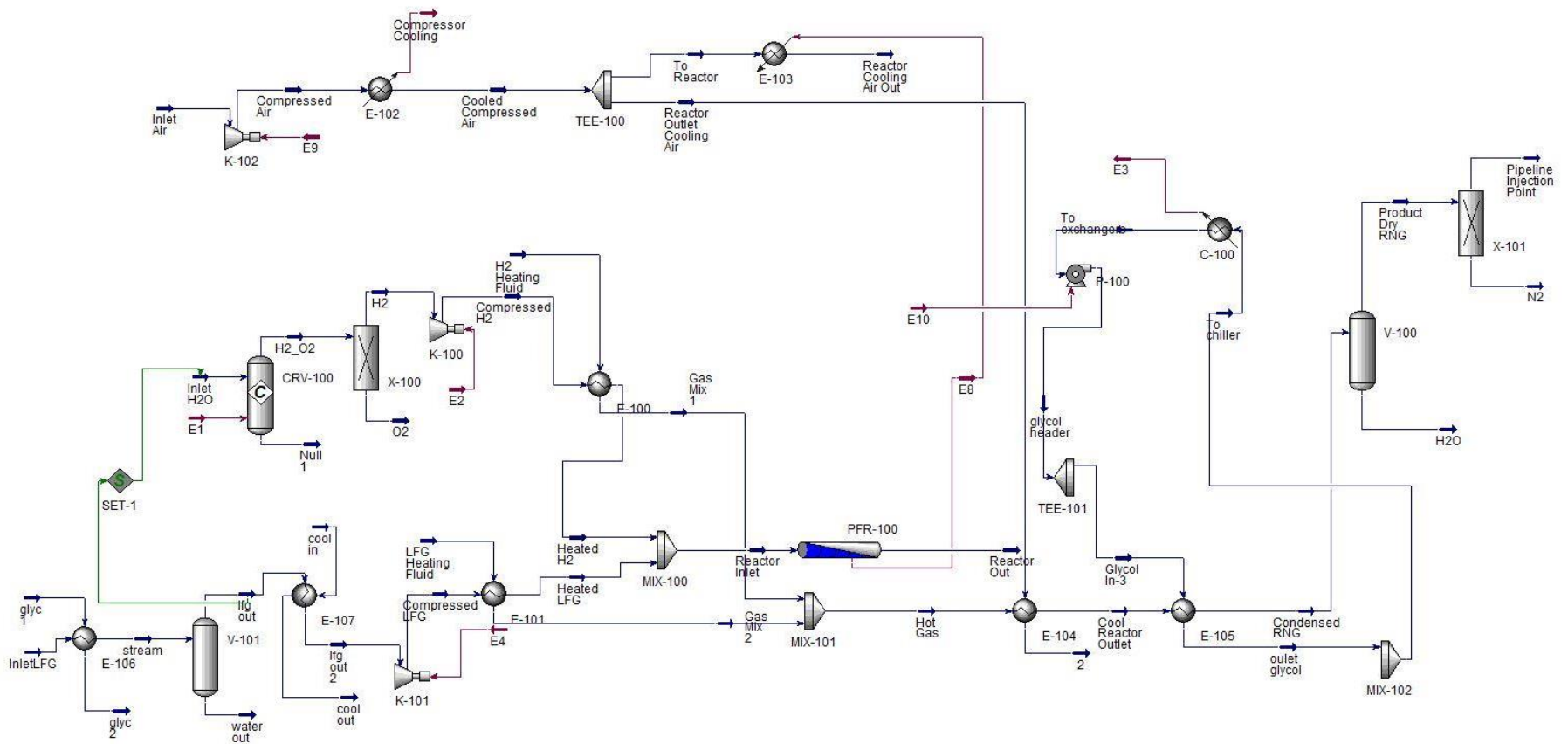
E. HYSYS Model

Figure 22. Aspen HYSYS SNG Facility Simulation Flowsheet

Table 9. HYSYS heat and material balance

	Unit	Inlet H2O	H2_O2	Null 1	H2	O2	Compressed H2	Heated H2	Dehydrated SNG	Water Outlet 2	Cooled Outlet 1	Pipeline Injection Point	N2
Vapour Fraction		0.00	1.00	0.00	1.00	1.00	1.00	1.00	1.00	0.00	1.00	1.00	1.00
Temperature	C	25.00	91.81	91.81	91.96	91.96	171.36	306.12	4.70	4.70	252.54	5.36	5.36
Pressure	kPa	600.00	600.00	600.00	600.00	600.00	1010.00	1006.93	987.04	987.04	999.09	987.04	987.04
Molar Flow	kgmole/h	444.50	666.73	0.00	444.50	222.24	444.50	444.50	409.26	204.74	312.00	278.99	130.27
Mass Flow	kg/h	8007.65	8007.65	0.00	896.11	7111.55	896.11	896.11	7557.22	3689.32	5714.85	4571.86	2985.36

	Unit	Inlet Air	Glycol Outlet 2	Glycol Feed 2	Cooled Reactor Outlet 2	Glycol Feed 3	Condensed SNG	Glycol Outlet 3	Compressed LFG	Heated LFG	Cooled Outlet 2	Reactor Cooling Air Out	Reactor Outlet H2 Heating Fluid
Vapour Fraction		1.00	0.00	0.00	0.84	0.00	0.67	0.00	1.00	1.00	1.00	1.00	1.00
Temperature	C	10.00	74.38	0.00	120.71	0.00	4.70	84.35	199.20	304.12	254.37	384.93	385.00
Pressure	kPa	111.46	194.15	200.00	993.92	200.00	987.04	192.94	1010.00	1004.46	997.29	200.00	1004.00
Molar Flow	kgmole/h	1500.00	800.00	800.00	614.00	800.00	614.00	800.00	372.90	372.90	302.00	1500.00	312.00
Mass Flow	kg/h	43425.00	32033.64	32033.64	11246.54	32033.64	11246.54	32033.64	10346.59	10346.59	5531.69	43425.00	5714.85

	Unit	Reactor Outlet LFG Heating Fluid	Cooled Reactor Outlet 1	Chilled Glycol	Cooled Compressed Air	Compressed Air	Reactor Inlet-2	Reactor Out-2	Reactor Inlet	Reactor Outlet	Inlet Sweet LFG	LFG Feed	LFG Cooled
Vapour Fraction		1.00	1.00	0.00	1.00	1.00	1.00	1.00	1.00	1.00	1.00	1.00	0.98
Temperature	C	385.00	253.44	0.00	27.00	139.06	300.00	385.80	304.69	384.66	45.00	35.00	5.00
Pressure	kPa	1004.00	997.29	180.00	300.00	310.00	1004.34	1003.69	1004.46	1003.80	250.00	270.00	260.00
Molar Flow	kgmole/h	302.00	614.00	1800.00	1500.00	1500.00	16.62	12.47	817.40	613.76	372.90	379.20	379.20
Mass Flow	kg/h	5531.69	11246.54	72075.69	43425.00	43425.00	229.09	229.09	11242.69	11242.60	10346.59	10459.90	10459.90

	Unit	Glycol Feed 1	Glycol Outlet 1	Dehydrated LFG	Water Outlet 1	Reactor Cooling Air Outlet HEF In	Reactor Cooling Air Outlet HEF Out	Heated Dehydrated LFG	Glycol Outlet Header	Chilled Glycol Header
Vapour Fraction		0.00	0.00	1.00	0.00	1.00	1.00	1.00	0.00	0.00
Temperature	C	0.00	30.31	5.00	5.00	384.90	327.96	45.00	74.11	0.00
Pressure	kPa	200.00	190.00	260.00	260.00	200.00	190.00	250.00	190.00	200.00
Molar Flow	kgmole/h	200.00	200.00	372.87	6.33	300.00	300.00	372.87	1800.00	1800.00
Mass Flow	kg/h	8008.41	8008.41	10345.70	114.20	8685.00	8685.00	10345.70	72075.69	72075.69

	Unit	E1	E2	E4	E9	E3	Compressor Cooling	E10	E8-2	E8
Heat Flow	kJ/h	1.29E+08	1014124	2154553	5601464	15477536	4892510.274	1723.526	322554.7	15995256